NASA Technical Paper 1504

Spatial-Frequency Response of the Limb Infrared Monitor of the Stratosphere

R. Gale Wilson, Antony Jalink, Jr.,
and William M. Kahlbaum, Jr.

AUGUST 1979

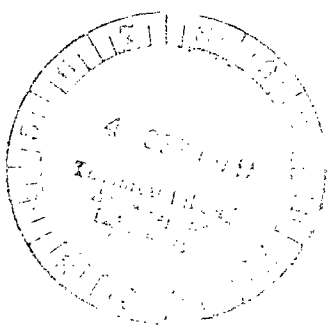

NASA Technical Paper 1504

Spatial-Frequency Response of the Limb Infrared Monitor of the Stratosphere

R. Gale Wilson, Antony Jalink, Jr.,
and William M. Kahlbaum, Jr.
Langley Research Center
Hampton, Virginia

National Aeronautics
and Space Administration

**Scientific and Technical
Information Branch**

1979

SUMMARY

The Limb Infrared Monitor of the Stratosphere (LIMS) is one of the experiments on the Nimbus-7 satellite. It is designed to scan the Earth's limb vertically and to measure spectral emission profiles of trace atmospheric gases that are believed to be important in processes controlling the stratospheric ozone distribution. The LIMS must have adequate spatial-frequency response for all the spectral channels to provide, through inversion of the measured limb radiance profiles, important information about the temperature, structure, and composition of the atmosphere. Experiment objectives are reviewed and several analyses and measurements are described which were performed to determine the adequacy of the system for satisfying these objectives. From the LIMS design-model data, the modulation transfer function (MTF) was calculated for the optical system, the detector field mask, the electronics, and the overall system for each channel. The signal output performance of the instrument was predicted from the system MTF data and model input radiance data for each channel. The MTF measurements made on the flight sensor confirmed the analytical results. The predictions indicate that the instrument can satisfy the basic measurement objectives of the experiment.

INTRODUCTION

The experiment Limb Infrared Monitor of the Stratosphere (LIMS), launched aboard the Nimbus-7 spacecraft in 1978, is designed to scan the Earth's limb vertically and to measure spectral emission profiles of trace atmospheric gases that are believed to be important in processes controlling the stratospheric ozone distribution. The limb radiance profiles of these gases (i.e., the spatial variation measured as the radiometer scans from the Earth's disk across the atmosphere) can be inverted (refs. 1 and 2) to provide important information about the temperature, structure, and composition of the atmosphere. The LIMS measures the radiance profiles of ozone (O_3), water vapor (H_2O), nitrogen dioxide (NO_2), nitric acid (HNO_3), and carbon dioxide (CO_2). The LIMS is one of several planned instruments (ref. 3) for surveying the atmosphere on a global scale and for obtaining an improved understanding of the physical and chemical relationships affecting its functions. The limited knowledge of the distributions of the gases within the atmosphere that LIMS will be measuring is due to natural variations such as latitude, season, and time, and to anthropogenic activities. For example, reference 4 provides a good survey of such variations for H_2O.

The specific experiment goals, system operation, and data-processing electronics of LIMS have been described in reference 5. The present paper elaborates on the spatial-frequency response characteristics of the LIMS and relates them to model radiance profiles of the type that the LIMS instrument is expected to observe. The limb-scanning technique used in the LIMS experiment, combined with the exponential falloff of atmospheric emission with altitude, provides an inherently high vertical-resolution potential (ref. 1).

Design and performance trade-off typically includes field of view, signal to noise, target radiance, instrument collection aperture, and spectral range, as well as science requirements.

After a brief review of the LIMS experiment objectives, the associated radiometric requirements and the analytical methods used to verify the optical-system design model are presented. Then analytical spatial-frequency response (modulation transfer function) data on the design model and the measured response data on the flight sensor are discussed. Finally, a brief assessment of the expected performance of the LIMS system is given, based on predicted inputs and on the system performance analysis.

Throughout the LIMS system analysis, the authors relied upon the computational expertise of William L. Edmonds, Systems and Applied Sciences Corporation.

LIMS EXPERIMENT OBJECTIVES

Measuring the stratospheric ozone distribution is the primary objective of LIMS. A typical radiance profile for O_3 has been synthesized from studies reported in references 6 and 7 and from related studies supporting the development of LIMS and earlier limb-scanning experiments (refs. 8 and 9). Typical radiance profiles have also been synthesized for H_2O, HNO_3, NO_2, and CO_2. The CO_2 radiance data, by virtue of the known uniform distribution of CO_2, allow determination of the atmospheric vertical temperature profile needed for inversion computations. Carbon dioxide has been extensively modeled from temperature and pressure profiles representing temporal, geographical, and meteorological variations over the Earth's surface (refs. 6 and 7). These models account for the absorption of water vapor and ozone in the outer portions of the CO_2 spectral band. Representative radiance profile models for the gases that LIMS measures are shown in figure 1. For the purposes of this paper, the spatial-frequency contents of the radiance profiles are primarily of interest (i.e., their Fourier spectra, estimations of which are shown in fig. 2). The radiance profiles are synthesized from 64 data points which correspond to 1-km increments of altitude; therefore, the maximum spatial frequency for which the spectra are determined is 0.5 cycle/km. It is seen that for all the profiles, the amplitude spectrum decays over the range defined by two or more orders of magnitude relative to the zero-frequency amplitude. The spectra were estimated by applying discrete Fourier transform techniques to the radiance profiles, after first multiplying the profiles by the Hann windowing function (ref. 10), followed by frequency averaging or smoothing (ref. 11).

The LIMS experiment seeks to provide radiance measurements with a 12-bit (4096-level) amplitude resolution and with an error not greater than ±1 percent for constant radiance (dc) targets. In addition, the measurements should have sufficient resolution to follow atmospheric features with a period as short as 5 km in altitude (i.e., a spatial frequency of 0.2 cycle/km at the

atmospheric target for four narrow instantaneous fields of view (IFOV's) and 0.1 cycle/km for two wide IFOV's). However, it is desirable that the instrument have the capability to respond to features of shorter period to determine whether they are present.

LIMS RADIOMETRIC SYSTEM

Figure 3 is a schematic of the LIMS optical system. The optical-system design was determined from a combination of resolution requirements, signal-to-noise constraints, and compatibility requirements set by the two-stage cryogenic cooler for the detectors (ref. 5). The system has three focal planes to satisfy the thermal and optical requirements. The first is located at the focus of the primary paraboloidal collector mirror, coincident with the chopper and calibration source (not shown in fig. 3). The second focal plane coincides with a thermal mask that is important in the cryogenic cooling requirements. The final focal plane contains band-pass filters, the field-defining stop, and the detectors. The following optical-system studies that are described relate to the final focal plane.

Figure 4 shows the shape of the field-stop mask and the corresponding detector array. The six detectors (four narrow and two wide) are located immediately behind the field stop. The detector dimensions are slightly larger than the field-stop apertures, so that all radiation within each IFOV is collected. The spectral band-pass filters are mounted on the front of the field stop. The atmospheric constituent corresponding to each detector is shown, as well as the wavelength value for each channel which was used in the optical-system analysis. Each wavelength in figure 4 is the midpoint of the LIMS channel spectral response. Because of the narrow spectral response of each LIMS channel, this midpoint corresponds essentially with the effective wavelength (centroid). Additional details of the LIMS optical system that are needed in the analyses are presented in appendix A.

The LIMS will determine the vertical distributions of stratospheric O_3, NO_2, HNO_3, H_2O, and temperature with resolutions of about 1 km for temperature, O_3, and HNO_3, and of about 2 km for NO_2 and H_2O. The CO_2 radiance profiles for the two pass bands become data input to inversion algorithms to determine the vertical temperature profile of the atmosphere (refs. 1 and 2). The inferred temperature profile is coupled with radiance data for the other gases to provide the distribution (density profile) of NO_2, H_2O, O_3, and HNO_3. The altitude ranges for measurements are from the troposphere to 75 km for temperature, to 64 km for O_3, to 50 km for H_2O, and to 40 km for HNO_3 and NO_2.

SPATIAL-FREQUENCY RESPONSE ANALYSIS

The prediction and evaluation of electro-optical systems performance by optical transfer function (OTF) techniques are now recognized procedures (ref. 12). The OTF calculations (predictions) based on the design parameters were performed for the LIMS optical system with two different computer programs for field angles corresponding to the geometric centers of the detectors. The two programs are POLYPAGOS (ref. 13) and ACCOS V (ref. 14). Before

comparative OTF calculations were done, agreement was established between the two programs for a paraxial ray-trace test case. For convenience, appendix B presents a brief tutorial on the analytical methods basic to these computer programs.

The OTF calculations for the LIMS optical system were made for the direction across the narrow dimension of the detector (i.e., along the vertical scan direction of LIMS). The modulation transfer function (MTF) data for two typical channels (O_3 and H_2O) of the LIMS that represent the two different IFOV's are shown in figures 5 and 6. The agreement between the two sets of independent LIMS (optics) MTF calculations appears consisent with the current state of the computational art for complex optical systems. (See appendix B.) The phase transfer function (PTF) is shown for all the channels in figure 7. The MTF data are presented for the range of spatial frequencies of primary interest in the LIMS application. More complete data are included in appendix C. Two spatial-frequency scales, cycles/mrad and cycles/mm, are shown. The two scales are related by

$$\frac{\text{cycles}}{\text{mrad}} \times \frac{1}{f} \times 10^3 = \frac{\text{cycles}}{\text{mm}} \tag{1}$$

where f is the focal length (157 mm) of the optical system. Later these spatial-frequency scales will be related to the cycles/km (at target), scale, in which performance requirements were specified.

The MTF curve for the HNO_3 channel (appendix C) is nearly the same as that for O_3. The MTF curves for the CO_2 channels (appendix C) are similar in shape to, but somewhat lower in magnitude than, the O_3 curves over most of the frequency range. The MTF curve for the NO_2 channel (appendix C) differs very little from that for the H_2O channel over the frequencies of most significance.

Appendix D presents methods used to define the best focal plane of the LIMS optical system. All the OTF data correspond to the best focus.

The overall system response function for each channel is defined by the product of (1) the optical transfer function, (2) the response characteristic due to the geometric subtense of the IFOV stop, and (3) the response of the filter in the signal-processing electronics. Figure 8 shows the predicted LIMS total electro-optical system MTF for the O_3 channel. In this figure, the curve designated MTF(O) is the optical system MTF, taken from figure 5 (ACCOS V data). The MTF(S) curve represents the field-stop (detector-slit) contribution, given by the relationship (normalized)

$$\text{MTF(S)} = \frac{\sin(\pi\beta f)}{\pi\beta f} \tag{2}$$

where β is half the IFOV (mrad) and f is the spatial frequency (cycles/mrad). The curve designated MTF(F) represents the response of the four-pole Butterworth filter, which provides a cutoff (3-dB) frequency of 4.4 Hz for the ozone channel, as well as for the CO_2 and HNO_3 channels.

For convenience, the frequency scale is given in three different units. The temporal-frequency scale (Hz) is related to the angular spatial-frequency (cycles/mrad) scale by the relationship

$$\text{Hz} = \frac{\text{cycles/mrad}}{\text{scan rate (mrad/sec)}} = \frac{\text{cycles/mrad}}{4.36 \text{ mrad/sec}} \tag{3}$$

The third frequency scale (cycles/km) is related to the cycles/mrad scale by the fact that 1 km at the target (Earth's horizon) subtends 0.286 mrad at the radiometer for the nominal orbital altitude of 900 km

$$\frac{\text{cycles}}{\text{km (at target)}} = \frac{\text{cycles} \times 0.286 \text{ mrad}}{\text{mrad km (at target)}} \tag{4}$$

The MTF coordinate is shown over a range of three decades. The two scales are related by

$$\text{dB} = 20 \log (\text{MTF}) \tag{5}$$

Figure 9 presents corresponding predicted LIMS total-system data for the H_2O channel. (See appendix C for similar results on the other four channels.) The detector-slit transfer function for the H_2O channel has a lower cutoff than that for the O_3 channel since the slit width for the H_2O channel is twice that for the O_3 channel. Also, the cutoff frequency of the electronics-filter function for the H_2O channel (NO_2 channel also (see appendix C)) is at a value one-half (i.e., 2.2 Hz) that for the O_3 channel (CO_2 and HNO_3 channels also). The overall system response for the NHO_3 channel is practically identical with that for O_3, and the system responses for the CO_2 channels differ insignificantly from the O_3 channel response. In addition, the NO_2 channel system response is practically identical with the H_2O channel response.

The dashed portions of the field-mask (slit) MTF curve (figs. 8 and 9) and of the system MTF curve represent the so-called "spurious resolution" regions of the system behavior beyond the first zero crossing of the field-mask transfer function. It is seen that the spurious resolution occurs at spatial frequencies greater than 0.57 cycle/km for the O_3 (CO_2 and HNO_3) channel and greater than 0.29 cycle/km for the H_2O and NO_2 channels. The values of 0.57 and 0.29 cycle/km in the object (target) plane correspond to the values of 2 cycles/mrad and 1 cycle/mrad, respectively (i.e., the first

zero points in the slit transfer functions). The LIMS MTF (spurious) beyond these two spatial frequencies is down by at least three orders of magnitude relative to the zero-frequency MTF.

The considerations in choice of the electronics-filter pass band are two-fold. On the one hand, the cutoff is chosen to pass all signal frequencies expected to be important. On the other hand, in the sampled data system used in LIMS (ref. 5), the location of the 3-dB frequency, together with the steepness provided by four poles, mitigates any aliasing error, as illustrated for the O_3 channel in figure 10. The figure shows the overall MTF for the O_3 channel folded about the sampling frequency of 41.7 Hz that is imposed by the LIMS Nimbus-7 data system. The logarithmic frequency scale distorts the mirror image. This figure indicates that aliasing errors are below the LIMS accuracy and resolution requirements since the overlap is nearly four orders of magnitude below the zero-frequency response.

Figure 11 shows the phase response of the overall LIMS system for all the channels. These curves reflect mainly the phase response of the Butterworth filter since the PTF of the optical system itself (fig. 7) is nearly zero for most of the channels over most of the frequency range.

MEASURED FREQUENCY RESPONSE

The amplitude responses of the LIMS radiometric channels (flight sensor) were measured by using a series of input square waves of constant amplitude and differing frequencies. The test setup is sketched in figure 12. A series of thermal bar targets, consisting of alternating heated and cooled metal bars, was placed in the focal plane of the test collimator. The cooled portion of the target (back plate) was kept at liquid-nitrogen temperature to maintain the required constancy of input amplitude. The temperature of the warm portions (plate with slots) was controlled at 300 $\pm$ 1 K by means of a circulating bath. The measured data on the LIMS O_3 channel show some typical results.

The response measured by means of the configuration shown in figure 12 is the square-wave response rather than the more conventional (sinusoidal input) MTF. The two responses can be compared by Fourier analysis. The response of the channel to the input square waves can be best understood by considering the following three frequency regions.

(1) For square-wave input frequencies from 0 to about 0.01 cycle/mrad, the O_3 channel responds with little amplitude and phase distortion. Therefore, the output closely resembles the input square wave. Figure 8 shows that the third and fifth harmonics suffer hardly any decrease in amplitude. Figure 11 shows that the phase shifts for the third and fifth harmonics of the 0.01 cycle/mrad square wave with respect to the fundamental are about 13° and 25°, respectively.

(2) For square waves in the range from 0.01 to 0.5 cycle/mrad, the output is distorted by increased phase shifts between the fundamental and harmonics. The phase shifts are caused mainly by the Butterworth filter. Phase shifts close to 180° between the fundamental and harmonics cause the resultant output wave to resemble a square wave with humps superimposed on it. The result is

that the maximum amplitude of the LIMS output for an input square wave in this frequency range is relatively larger than that for input waves in the lower frequency range.

(3) For input frequencies greater than 0.5 cycle/mrad, the phase shift between the fundamental and harmonics decreases rapidly with increasing spatial frequency, but here the effects of steeply falling LIMS amplitude (sinusoidal) response suppress contributions of these harmonics almost completely. Consequently, for the higher frequencies, the output is a nearly sinusoidal response (i.e., a sinusoidal output is obtained for a square-wave input).

The measured responses representing the three frequency regions previously discussed for the LIMS O_3 channel are shown in figure 13. The expected distortions discussed are apparent in these measurements. The LIMS output response was characterized by determining the peak-to-peak amplitude of the output waves, which was then divided by the response for a zero-frequency target. These results are shown in table I for all the LIMS channels for spatial frequencies from 0 to 1.2 cycles/mrad.

The peak-to-peak measured square-wave response data for the ozone channel, corresponding to the data in table I, are shown in figure 14 as a series of circles. The solid-line curve, reproduced from figure 8, is the MTF predicted for the O_3 channel from design data. The dashed curve represents the peak-to-peak square-wave amplitude response predicted from the ozone channel by the Fourier analysis considerations previously described. Peaking of the dashed curve in the midfrequency range occurs because of superposition and relative phase shifts of the square-wave harmonics. The measured response reflects a small increase in the midfrequency range, consistent with that predicted for square-wave inputs, and then a gradual decrease to sinusoidal-output behavior. However, the measured data (circles in fig. 14) are below the predicted square-wave response curve, consistent with the fact that system manufacturing and alignment errors would be expected to reduce the performance as compared with that of idealized predictions. The channel retains close to 30 percent of the zero-frequency response at the $1/(2 \times \text{IFOV})$ frequency (1 cycle/mrad) to reflect the proper trade-off with field-mask (slit) dimensions.

PREDICTED FOURIER SPECTRUM OUTPUT AMPLITUDE

To obtain the predicted output of LIMS for each channel, normalized to the zero-frequency output, the following relationship is used:

$$\text{Output spectrum} = \text{MTF(LIMS)} \times \text{input spectrum} \qquad (6)$$

This relationship applies because there is a spatially incoherent radiance input to the optical system (including field mask) which linearly maps object radiance into image irradiance at the detectors. The electronic system, in turn, linearly maps the irradiance into a voltage output, its transfer function being that of the Butterworth filter (figs. 8 and 9).

Figure 15 presents the predicted normalized LIMS Fourier spectrum output amplitudes for all channels of the radiometer as determined from equation (6) (i.e., from multiplying the calculated MTF by the predicted input spectrum amplitude for each channel (fig. 2)). These predictions indicate that, for the H_2O and NO_2 channels, the output spectrum magnitude (relative to the zero-frequency output) at 0.286 cycle/km, where the resolution becomes spurious, would be less than 10^{-5}. For the O_3 and HNO_3 channels, the output spectrum magnitude at 0.572 cycle/km, where the resolution becomes spurious, would be about 2×10^{-5} and 10^{-5}, respectively. The CO_2 channel output at 0.572 cycle/km appears to be less than 10^{-6} because its spectral falloff is faster than that for the other narrow IFOV channels. These predicted outputs are based on some extrapolation beyond the spectral range of the input-spectrum calculations, as indicated by the dashed parts of the curves in figure 15. The implications are that any spurious resolution would be indistinguishable from noise unless the system could accurately quantize more than 50 000 radiance levels.

As stated earlier, the LIMS experiment seeks to provide radiance-measurement capability, with an amplitude resolution of 12 bits, at spatial frequencies at the atmospheric target up to 0.2 cycle/km for the narrow IFOV's and up to 0.1 cycle/km for the wide IFOV's. Nominal variations of the instrument temperature in orbit cause changes in the self-radiation of the optical system, to which the infrared detectors are sensitive. To prevent possible saturation of the channels due to variations in the optical-system radiation component, the full-scale radiance excursion (midrange) of each channel is set to 80 percent of the full 12-bit (4096-level) data-system range or to 3276 quantization levels (counts). Therefore, the operational requirement on amplitude resolution becomes one part in 3276, or 3.1×10^{-4}, up to 0.10 cycle/km for the NO_2 and H_2O channels, and up to 0.20 cycle/km for the O_3, CO_2, and HNO_3 channels. As seen in figure 15, the predicted LIMS output magnitudes at these spatial frequencies, normalized to zero-frequency output, are 5.4×10^{-2} for NO_2, 4.3×10^{-2} for H_2O, 2.6×10^{-3} for O_3, 4.1×10^{-4} for CO_2, and 3.1×10^{-3} for HNO_3. Therefore, the predicted outputs for all the channels are greater than the required amplitude resolution at the highest spatial frequencies of interest by factors ranging from slightly more than 1 for the CO_2 channel to 174 for the NO_2 channel. These predicted outputs indicate the LIMS performance is adequate, provided the noise levels for all the channels are also less than the required amplitude resolution. Data that have become available since the October 1978 launch of Nimbus-7 (personal communication with John C. Gille, National Center for Atmospheric Research, and James M. Russell III, Langley Research Center, who were principal co-investigators for the LIMS experiment) show the typical noise levels relative to the maximum channel range are 3.8×10^{-4} for NO_2; 4.2×10^{-4} for H_2O; 4.6×10^{-5} for O_3; 8.9×10^{-5} for CO_2(wide); 3.6×10^{-4} for CO_2(narrow); and 7.0×10^{-5} for HNO_3. The noise levels represent the total spatial-frequency bandwidth of each channel. The noise levels appropriate to the 0.10 cycle/km (NO_2 and H_2O) and the 0.20 cycle/km (O_3, CO_2, and HNO_3) frequencies would be much further reduced by the effects of the electronics MTF on the noise spectrum.

CONCLUDING REMARKS

Experiment objectives of the Limb Infrared Monitor of the Stratosphere have been reviewed and related to its predicted and measured spatial-frequency response. Consideration of the predicted output signal spectrum and the flight-observed noise levels together indicates very favorable signal-to-noise characteristics up to the highest significant spatial frequencies.

Langley Research Center
National Aeronautics and Space Administration
Hampton, VA 23665
June 8, 1979

APPENDIX A

LIMS OPTICAL SYSTEM

Figure A1 repeats the LIMS optical-system schematic shown in figure 3 but breaks it into three parts to show all the important construction parameters needed for the optical transfer function (OTF) calculations. Figure A1(a) shows the front-end elements, including the first lens, and figure A1(b) shows the remainder of the system, with the first lens also included. Figure A1(c) shows details of the last lens in the system and of the focal-plane assembly (i.e., the spectral filters, field mask, and detectors). The field mask that defines the instantaneous field of view (IFOV) for each channel was shown in figure 4. The view of the field mask shown is along the optical axis Z (i.e., perpendicular to the view in fig. A1(c)). The field-mask configuration is symmetric about the X- and Y-axes.

Table AI shows the refractive indexes at the appropriate temperatures (see fig. 3) and wavelengths for the CdTe lenses and window and for the Ge substrates of the spectral band-pass filters. These index data, along with the temperature data in figure 3 and the information in figures 4 and A1, provide all the necessary inputs for calculating the OTF of all channels of LIMS.

TABLE AI.- INDEX OF REFRACTION

Wavelength, μm	Index of refraction for -			
	CdTe(Irtran-6)[1] at temperature, K, of -			
	297.5	152	65	Ge at 65 K
6.21 (NO_2)	2.68499	2.67115	2.66288	3.91743
6.83 (H_2O)	2.68332	2.669533	2.661294	3.915565
9.64 (O_3)	2.67621	2.66236	2.65409	3.91131
11.32 (HNO_3)	2.67139	2.65755	2.64927	3.91028
15.20 (CO_2 wide)	2.65751	2.64390	2.63575	3.90934
15.23 (CO_2 narrow)	2.65751	2.64390	2.63575	3.90934

[1]Irtran-6: Registered trademark of Eastman Kodak Company.

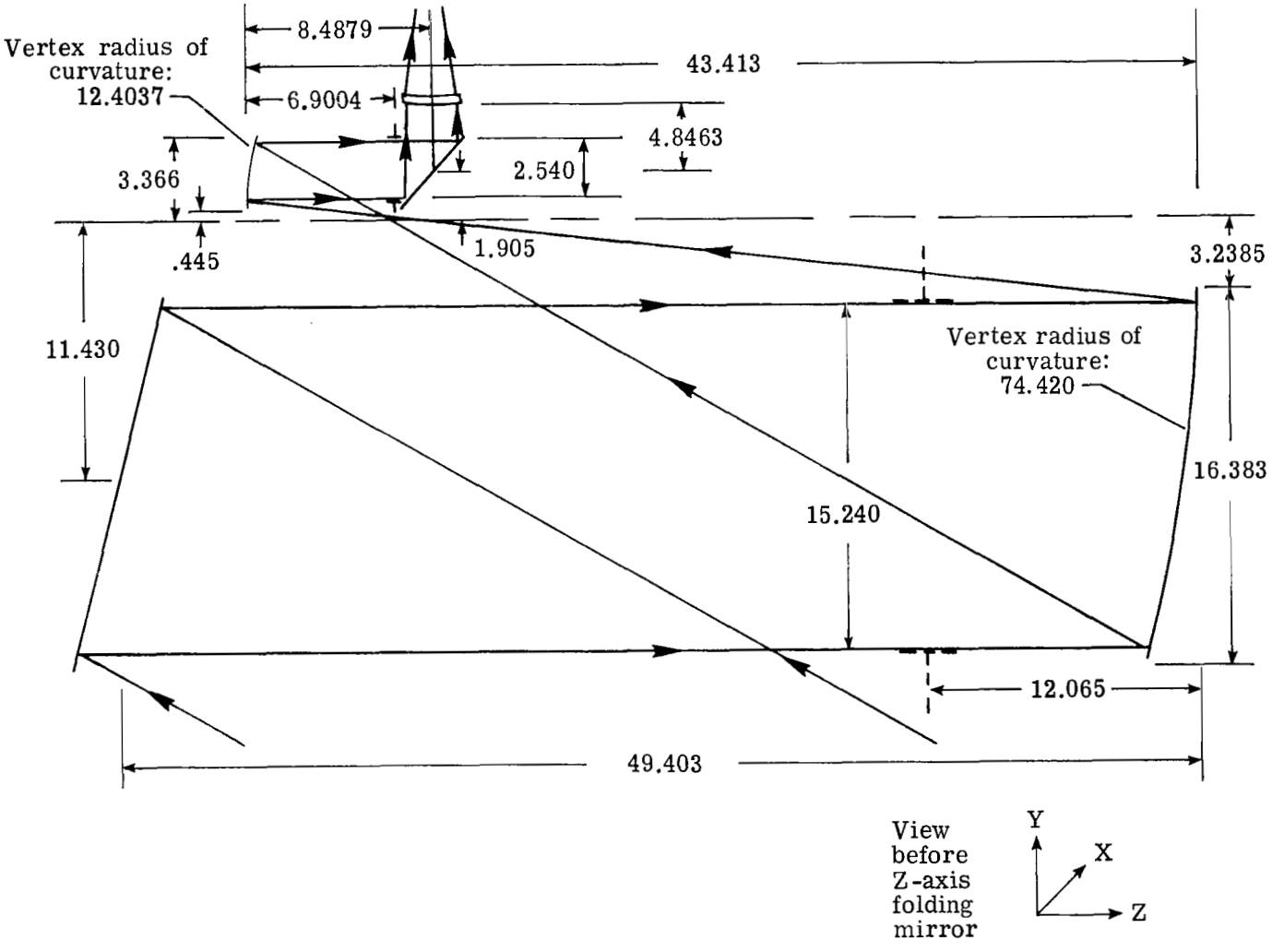

(a) Input end.

Figure A1.- LIMS optical-system schematic. All dimensions are given in centimeters.

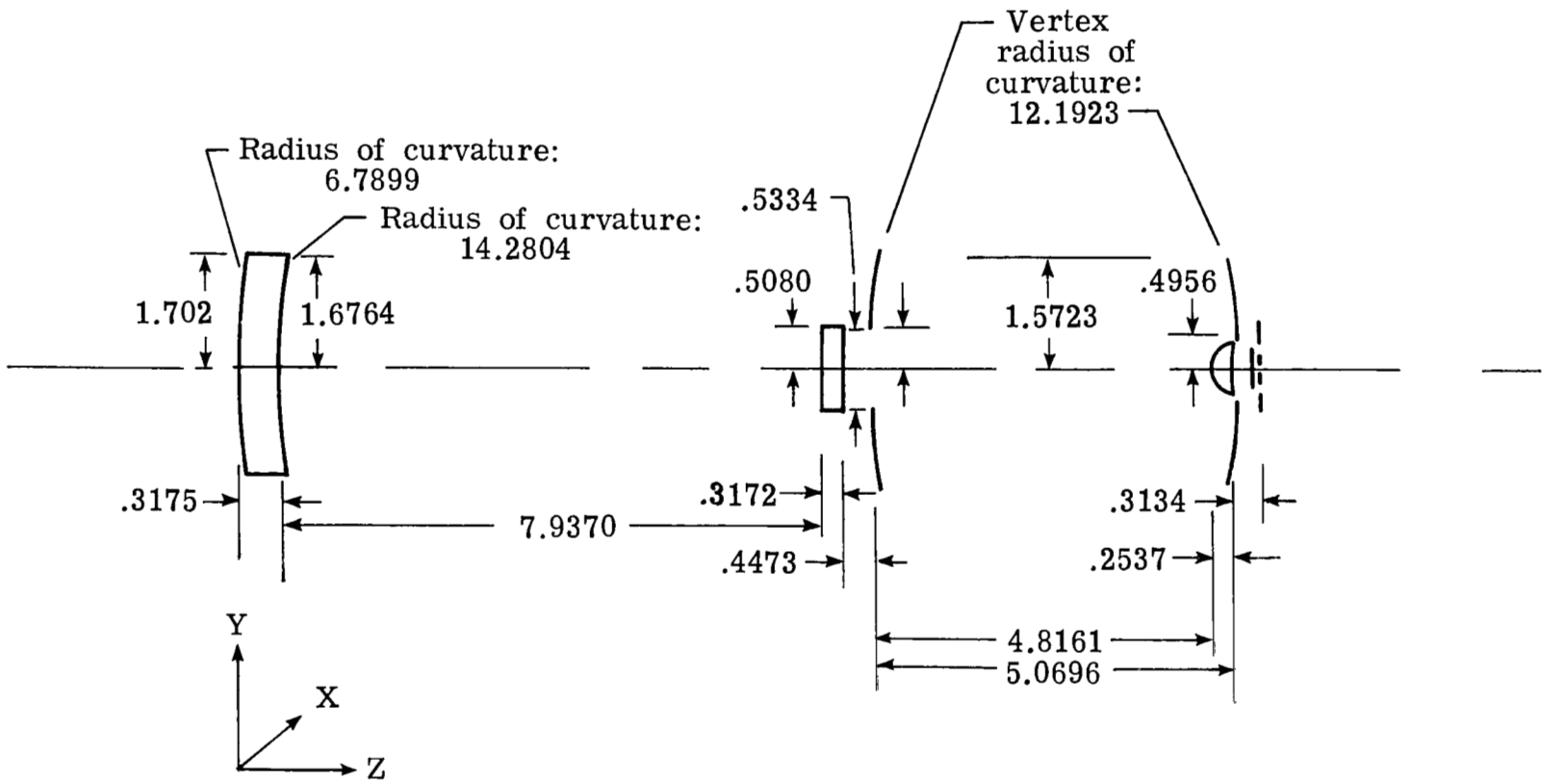

(b) Output end.

Figure A1.- Continued.

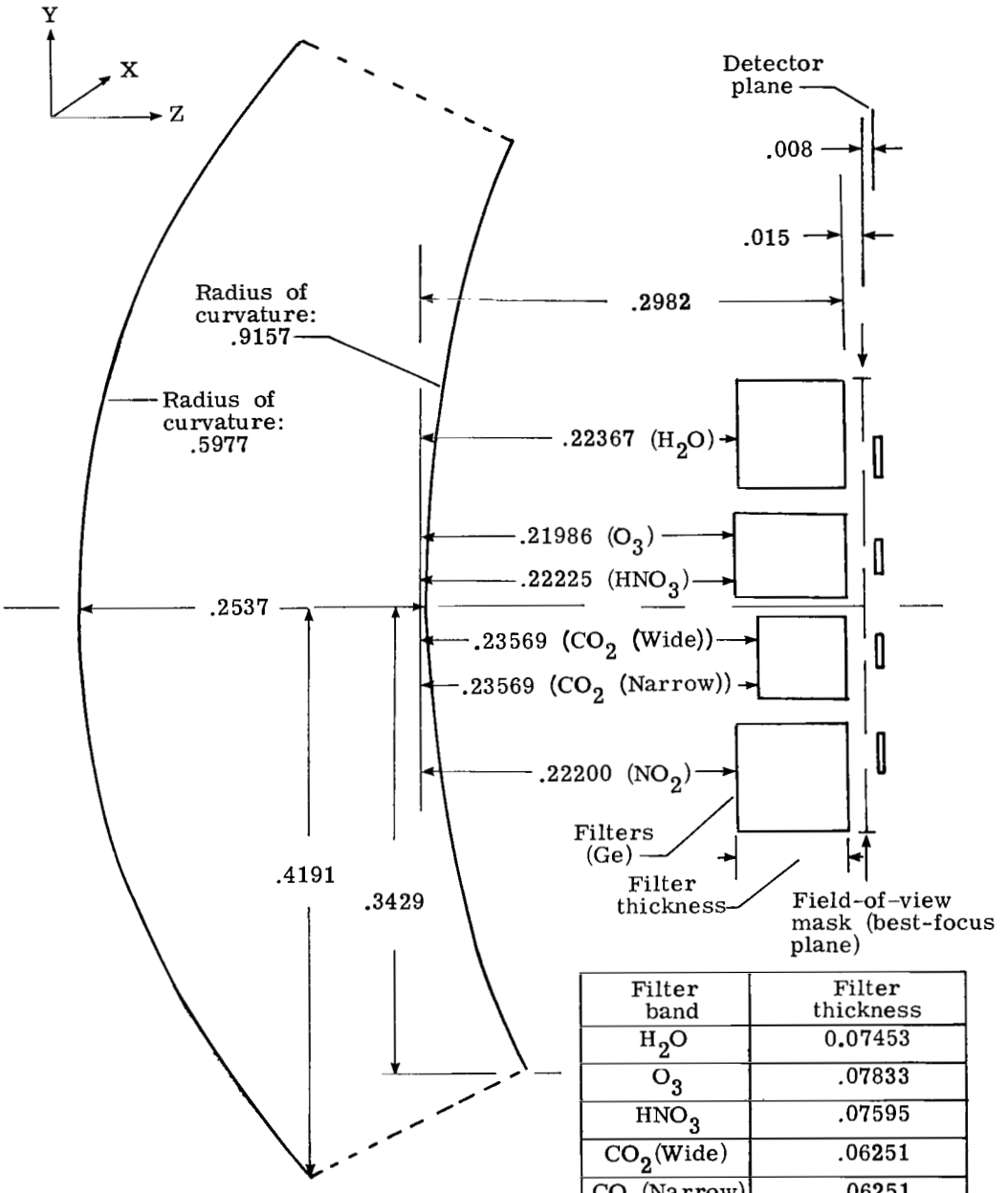

Filter band	Filter thickness
H_2O	0.07453
O_3	.07833
HNO_3	.07595
CO_2(Wide)	.06251
CO_2(Narrow)	.06251
NO_2	.07620

(c) Focal-plane assembly.

Figure A1.- Concluded.

APPENDIX B

ANALYTICAL METHODS FOR OPTICAL TRANSFER FUNCTION CALCULATIONS

Although the calculation of the optical transfer function (OTF) from optical design parameters is, in principle, a straightforward matter, many approximations and simplifying assumptions are required, in practice, to make the numerical calculations manageable. Different analysts and designers make different compromises in their computer programs and generally get somewhat different results. Only recently have these differences been well enough understood to provide good agreement between results obtained by different evaluators and to assure good reproducibility among results of an individual evaluator (refs. 12, 15, and 16).

POLYPAGOS Computer Program

POLYPAGOS (currently named the Spectral Lens Analysis Program (SLAP) and developed by the Pagos Corporation) is a general-purpose program for analysis of complex optical systems. Specific mathematical details can be found in references 13, 17, and 18, and background treatments can be found in such textbooks as references 19 and 20. With POLYPAGOS and similar programs, the first step in the analysis of a system is the computation of the pupil function by suitable ray-tracing procedures. The pupil function describes the combined effects of diffraction (system limiting aperture) and aberrations on the otherwise ideal wavefront propagated through the system.

Fourier transformation of the pupil function yields the amplitude spread function (ASF), and the point spread function (PSF) is obtained from $\mathrm{PSF} = |\mathrm{ASF}|^2$. Physically, the PSF is the diffraction pattern or optical power spectrum in the image plane for a point-source object (input), as would be measured with a square-law detector such as photographic film or a photodetector. The OTF which results from a Fourier transformation of the PSF is a two-dimensional complex function that may be written

$$\mathrm{OTF} = R(f_x,f_y) + iI(f_x,f_y) \tag{B1}$$

where R and I represent the real and imaginary parts and f_x and f_y are spatial-frequency variables for the x- and y-directions. The OTF must be specified for a given field position, for a given direction, and for a given wavelength unless a polychromatic quantity is determined by averaging.

The phase transfer function (PTF) is given by

$$\phi = \tan^{-1}\left[\frac{I(f_x,f_y)}{R(f_x,f_y)}\right] \tag{B2}$$

and the modulation transfer function (MTF) by

$$MTF = \left[R^2(f_x,f_y) + I^2(f_x,f_y)\right]^{1/2} \tag{B3}$$

The meanings of MTF and PTF are best understood by considering that a given distribution of radiance in the object plane of an optical system can be considered as arising from the superposition of sine-wave grating distributions of radiance of different spatial frequencies, phases, orientations, and amplitudes. The distribution of irradiance in the image can be built up from sinusoids in the same way. The MTF is the variation with spatial frequency of the ratio of the contrast in the sinusoidal image that is produced to the contrast of a sinusoidal test object.

The PTF is a measure of the lateral displacement of the component sinusoids from the origin of the image coordinate system; it is measured in radians or other angular units, where 2π radians are equivalent to one period of the image of the sinusoidal test object. The PTF is the least understood aspect of the OTF. Reference 15 (pages 39-43) shows that the meaning of the PTF is always ambiguous unless the PSF is evenly symmetrical. Therefore, the practical importance of the PTF in image evaluation is still to be fully resolved. A linear phase shift just translates the diffraction image without detrimental effect on the image quality. Programs such as POLYPAGOS provide for automatic removal of linear phase shifts. Nonlinear phase shifts, however, introduce harmonic distortion that results in serious deterioration of image quality.

ACCOS V Computer Program

The ACCOS V program is a comprehensive program including optimization routines for use in designing and evaluating a broad range of optical systems. The ACCOS V program derives the OTF by autocorrelation of the pupil function, a process mathematically equivalent to the Fourier transformation operations of the POLYPAGOS program. However, if the full two-dimensional OTF is not required, the autocorrelation process is more computationally efficient than the Fourier transform process.

APPENDIX C

SUPPLEMENTARY MODULATION TRANSFER FUNCTION DATA ON LIMS RADIOMETRIC SYSTEM

In the main text of this report, modulation transfer function (MTF) data were presented on the O_3 and H_2O LIMS channels over the spatial-frequency range of primary significance in the LIMS application (figs. 5 and 6), and the close similarities of data on the other channels to these two data sets were discussed. In this appendix, additional MTF data for all six channels are presented for spatial frequencies up to about the cutoff spatial frequency of the optical system for the CO_2 wavelength. The data might be of interest (perhaps aside from the LIMS application) in the frequency response of a LIMS-type radiometric system. These results are contained in figures C1 to C6.

In addition to calculations of MTF at field angles corresponding to centers of the detectors (represented by the data points in figs. C1 to C6), MTF values were calculated for field angles corresponding with the detector extremities (see circular dots on detectors in fig. 4); the extremity values of MTF are represented in figures C1 to C6 by the ends of the vertical bars. The spread (y-direction) in MTF values for different field angles along the length (x-direction) of each detector is due to the variation in aberrations with increased or decreased field angle.

The differences between the POLYPAGOS and ACCOS V MTF results may be accounted for through the considerations of the first paragraph of appendix B. However, the differences are not very significant relative to the final system MTF results (i.e., the MTF (LIMS) curves in figs. 8 and 9 and figs. C7 to C10).

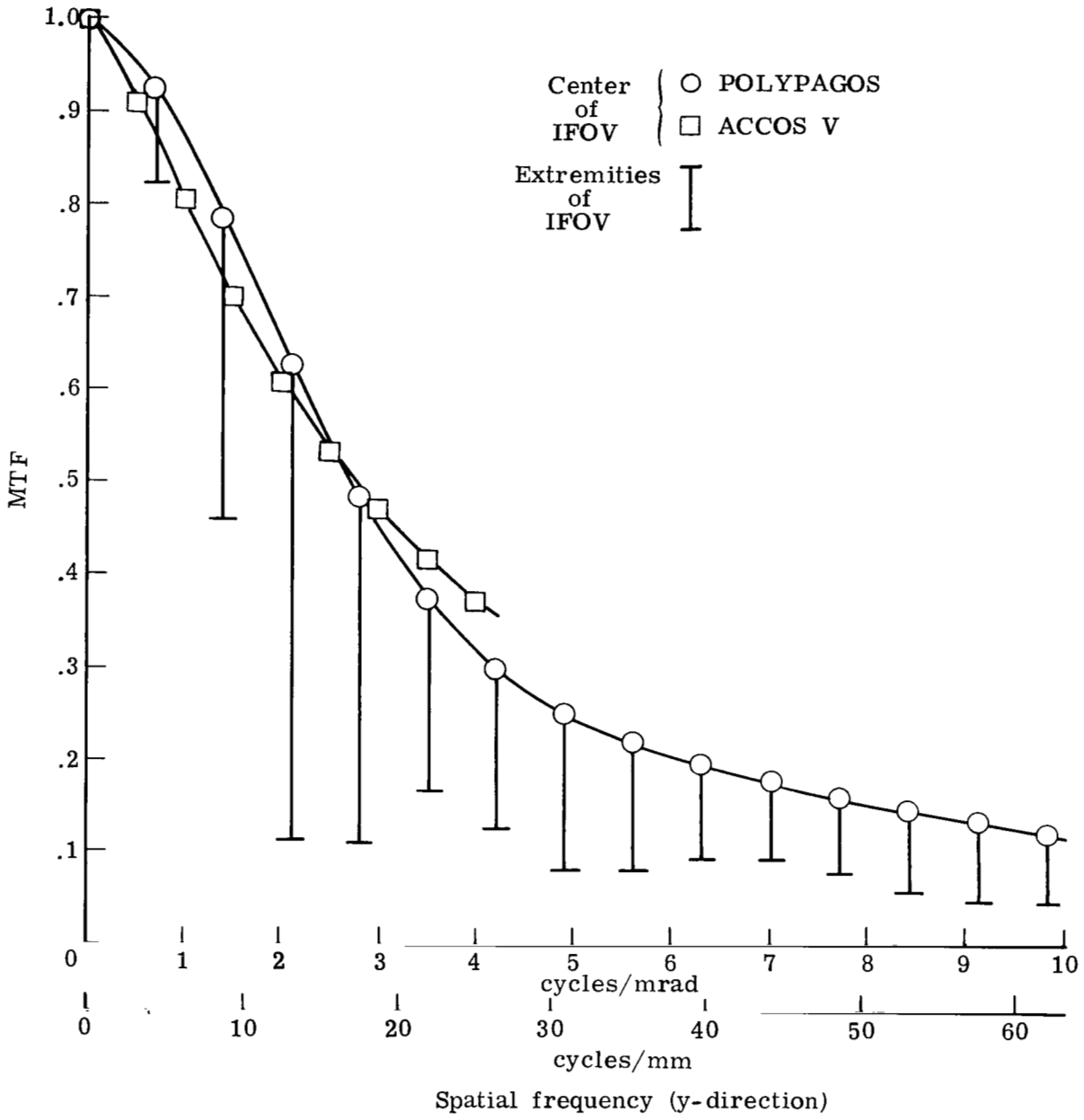

Figure C1.- MTF(optics) of LIMS NO_2 channel.

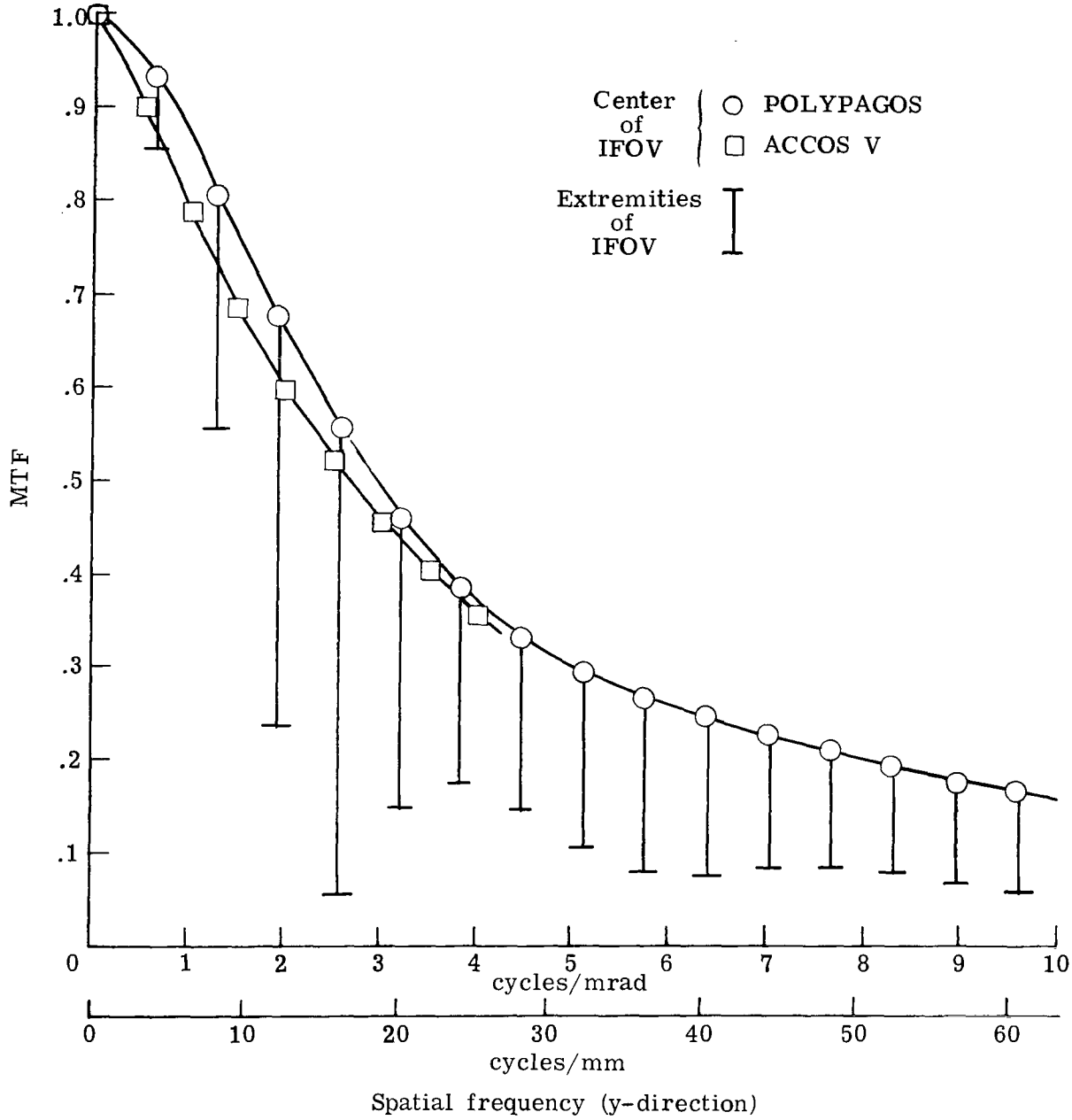

Figure C2.- MTF(optics) of LIMS H_2O channel.

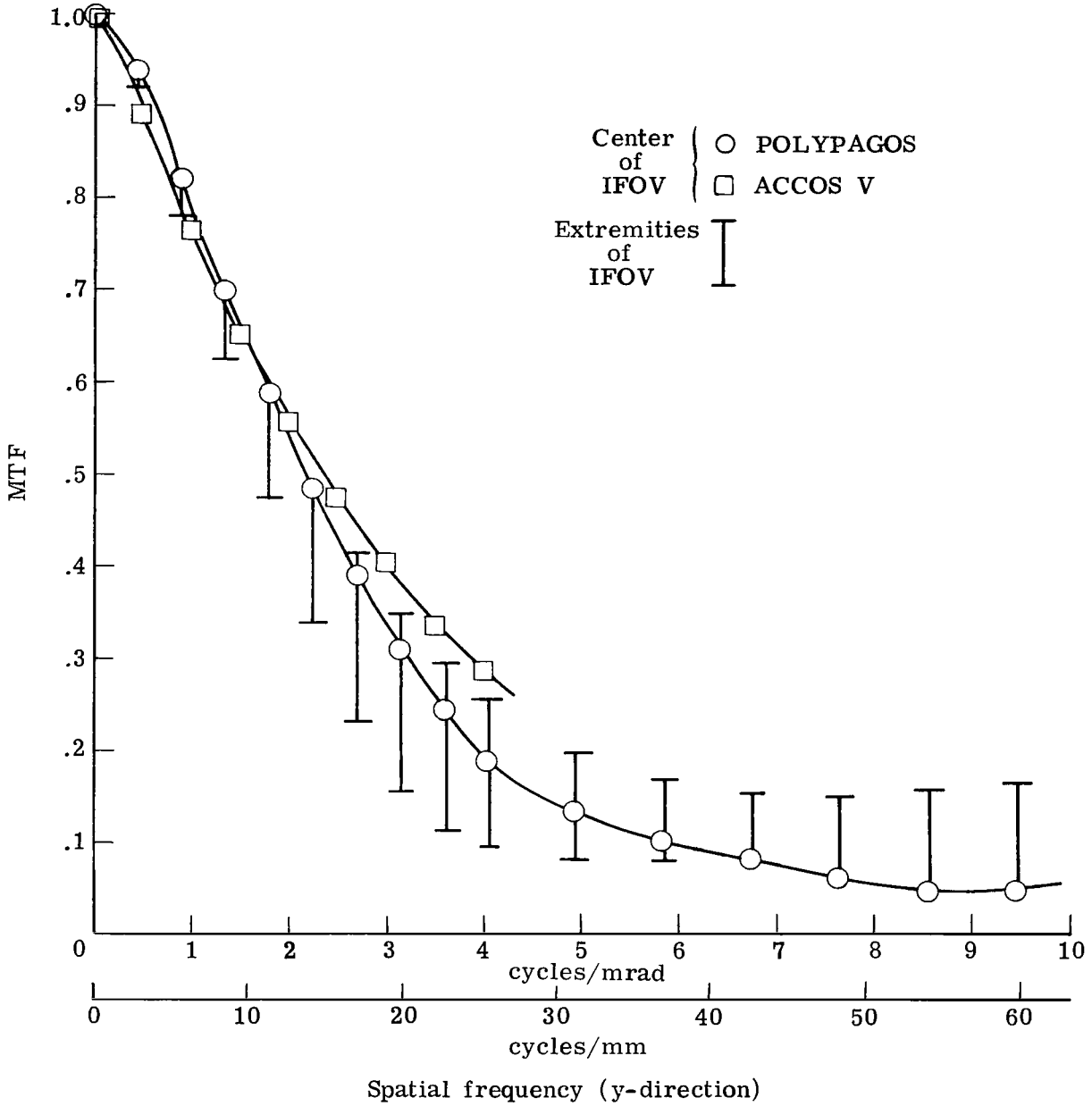

Figure C3.- MTF(optics) of LIMS O_3 channel.

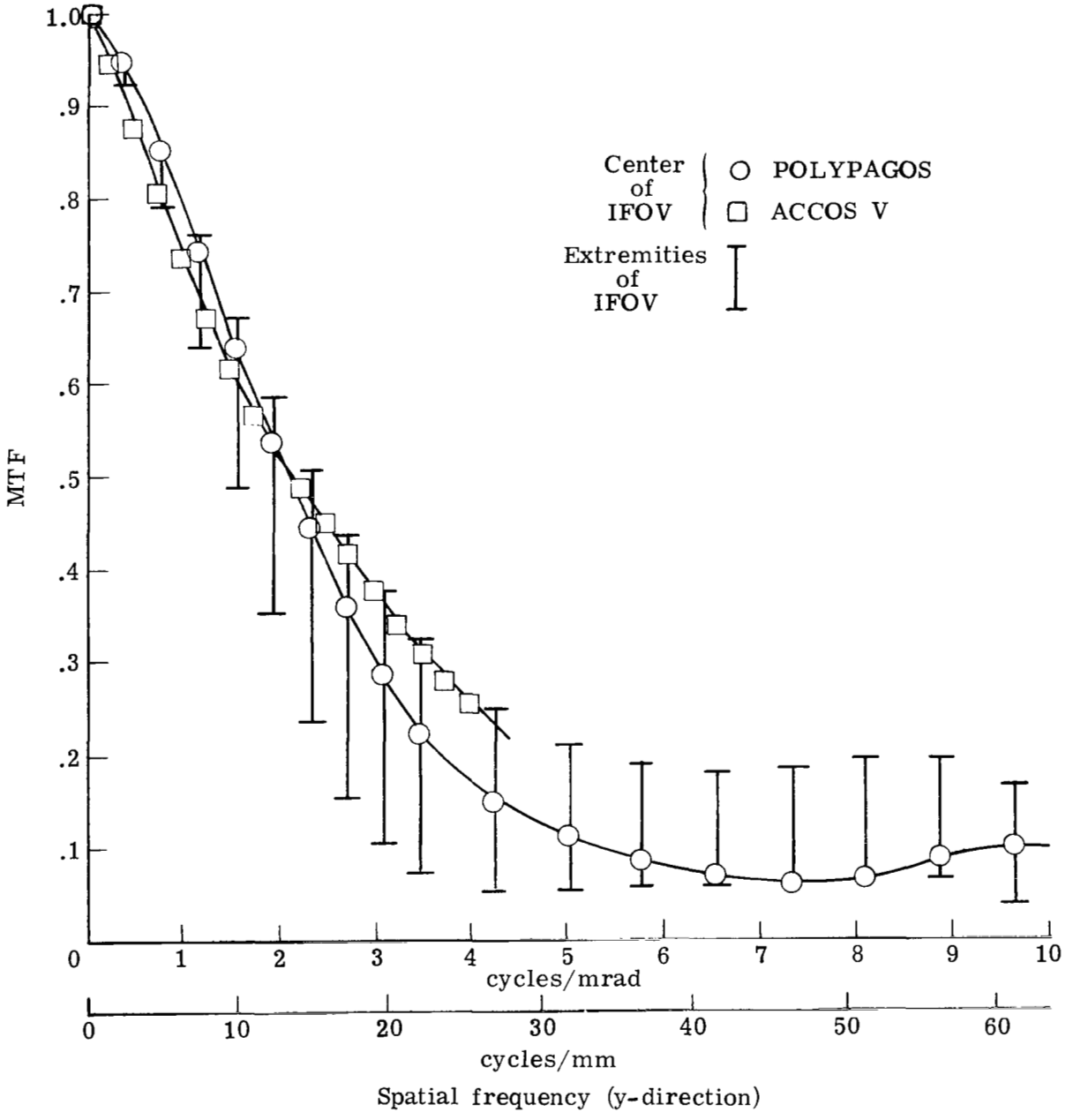

Figure C4.- MTF(optics) of LIMS HNO_3 channel.

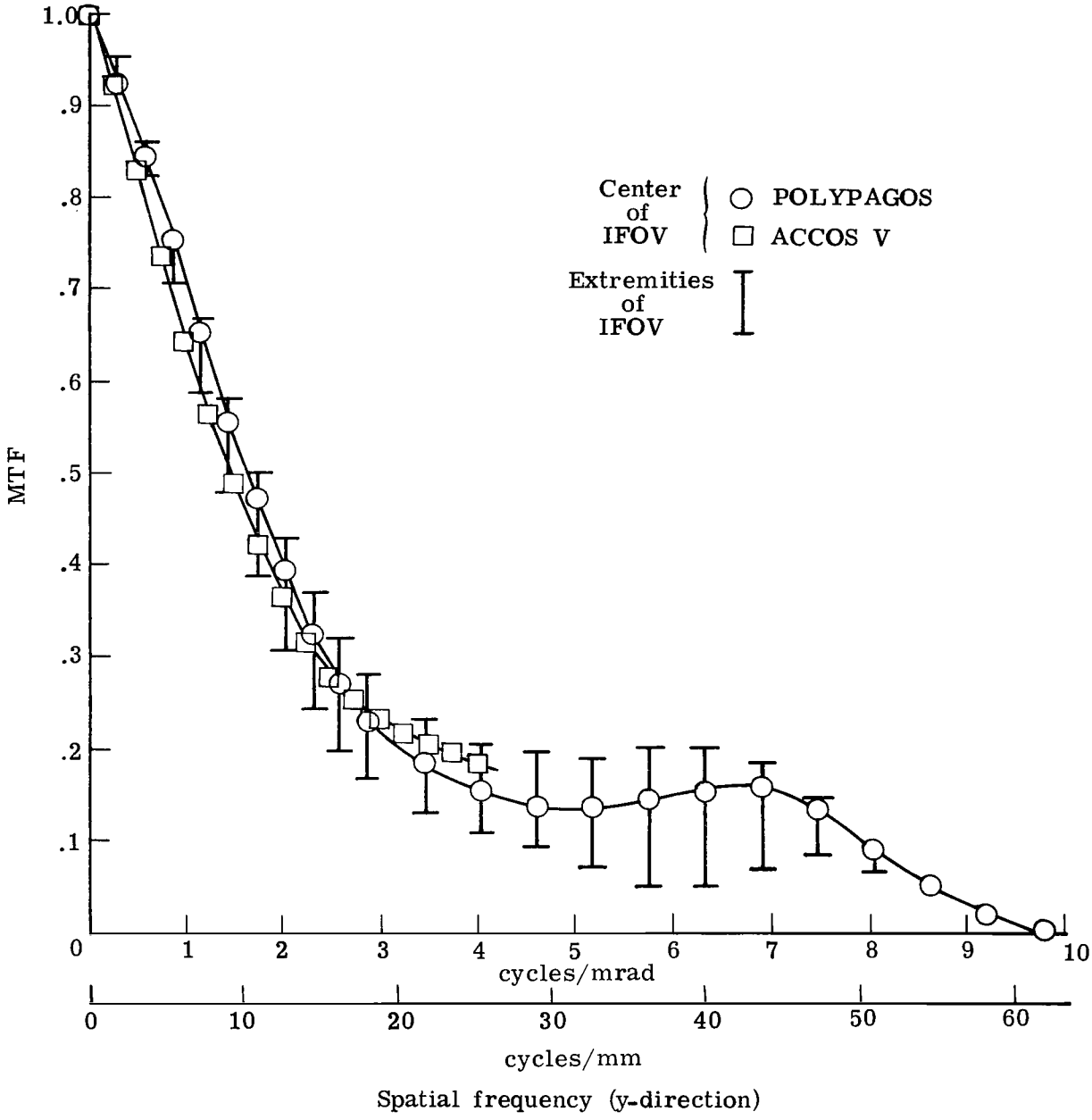

Figure C5.- MTF(optics) of LIMS CO_2(wide) channel.

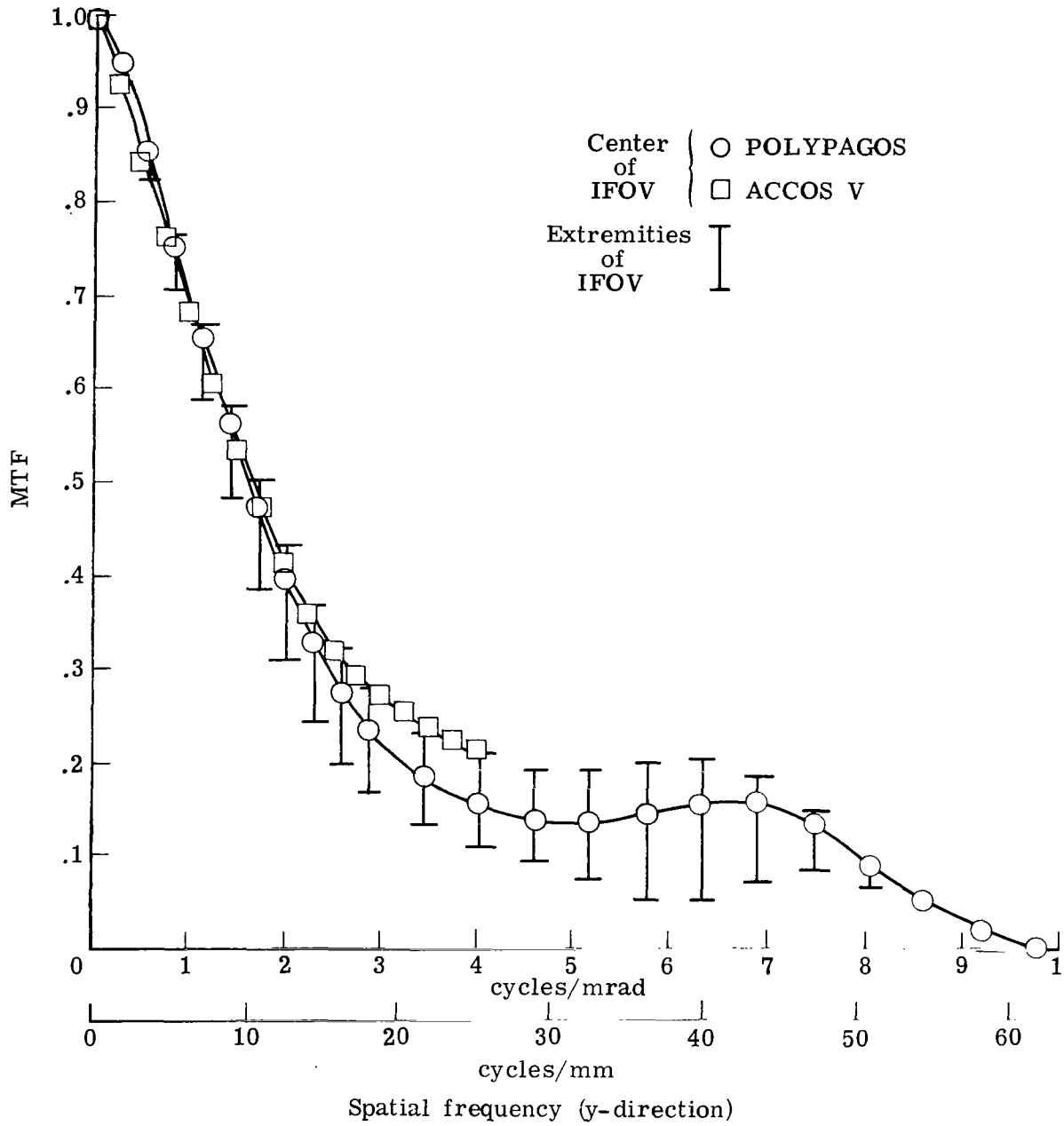

Figure C6.- MTF(optics) of LIMS CO_2(narrow) channel.

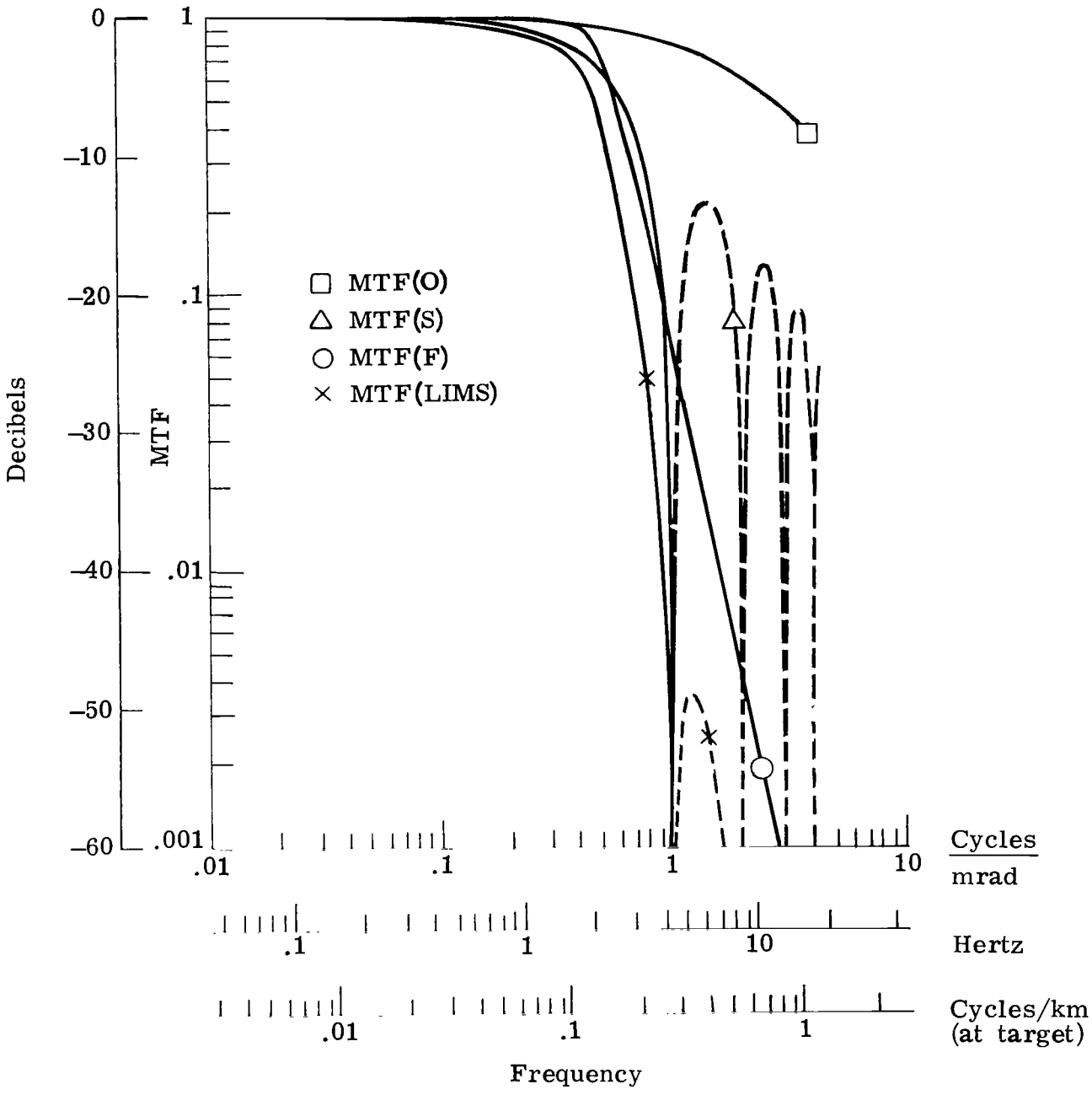

Figure C7.- Frequency response of LIMS radiometer for NO_2 channel. Dashed curve indicates spurious resolution.

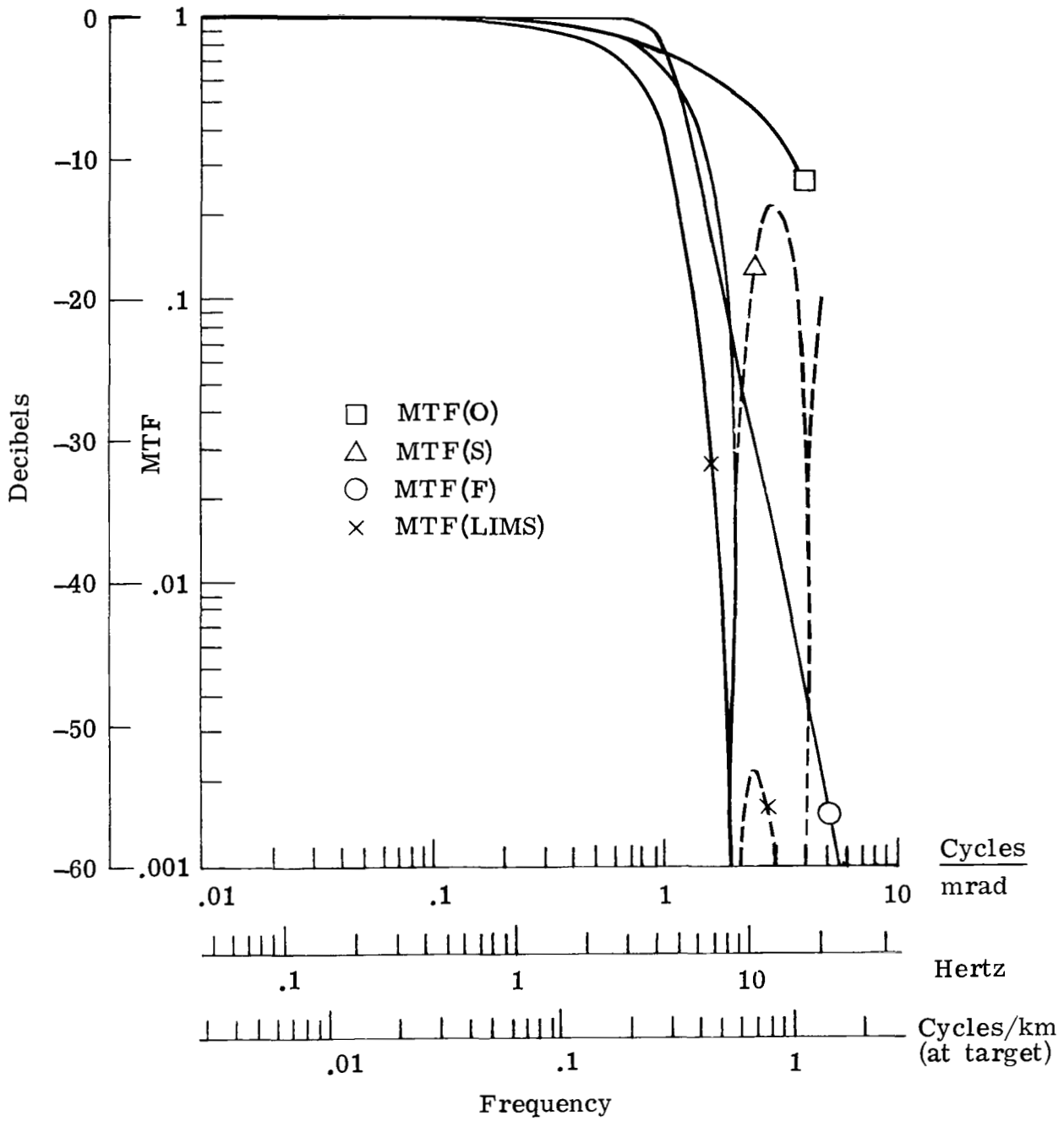

Figure C8.- Frequency response of LIMS radiometer for HNO_3 channel. Dashed curve indicates spurious resolution.

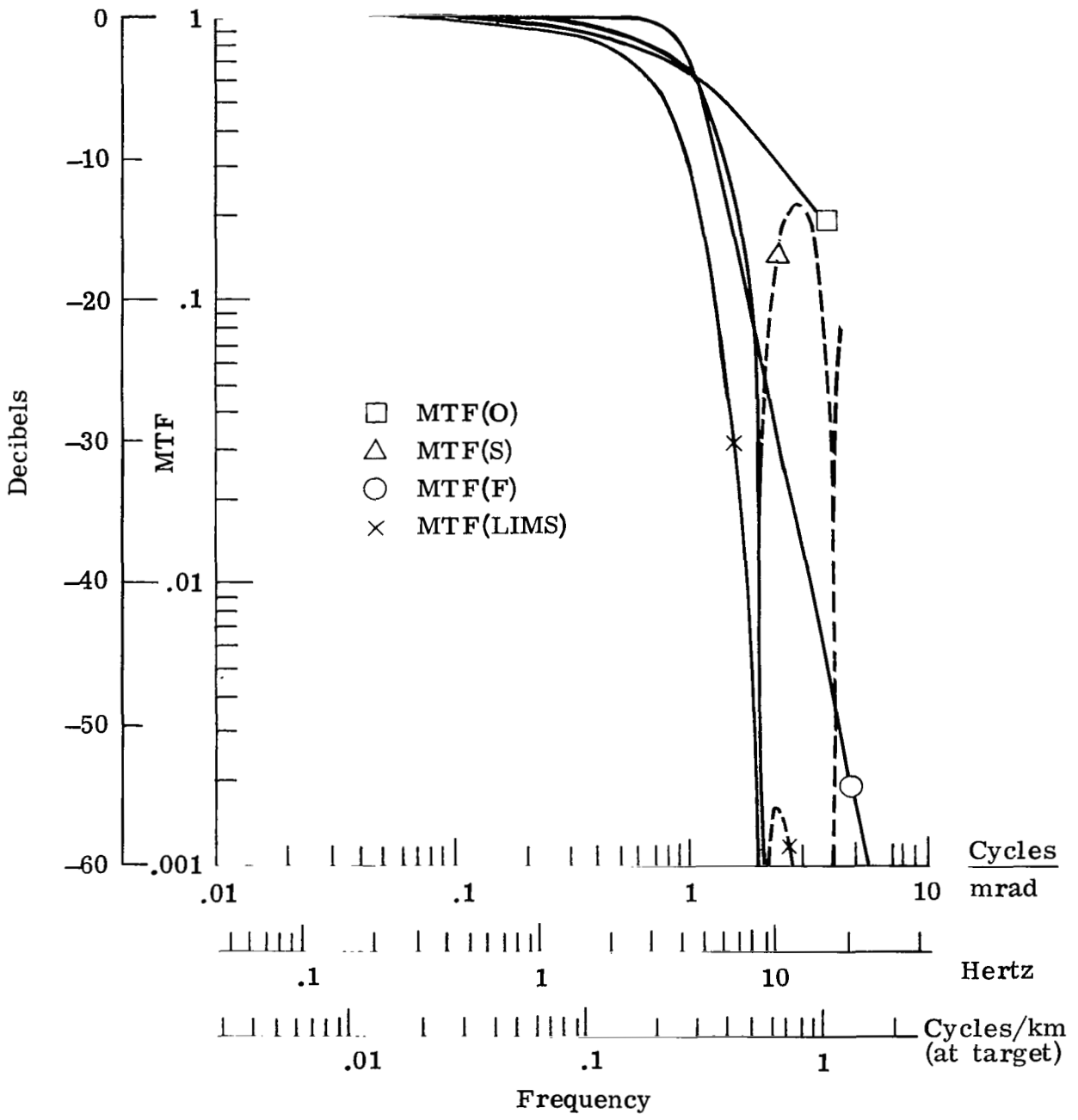

Figure C9.- Frequency response of LIMS radiometer for CO_2(wide) channel. Dashed curve indicates spurious resolution.

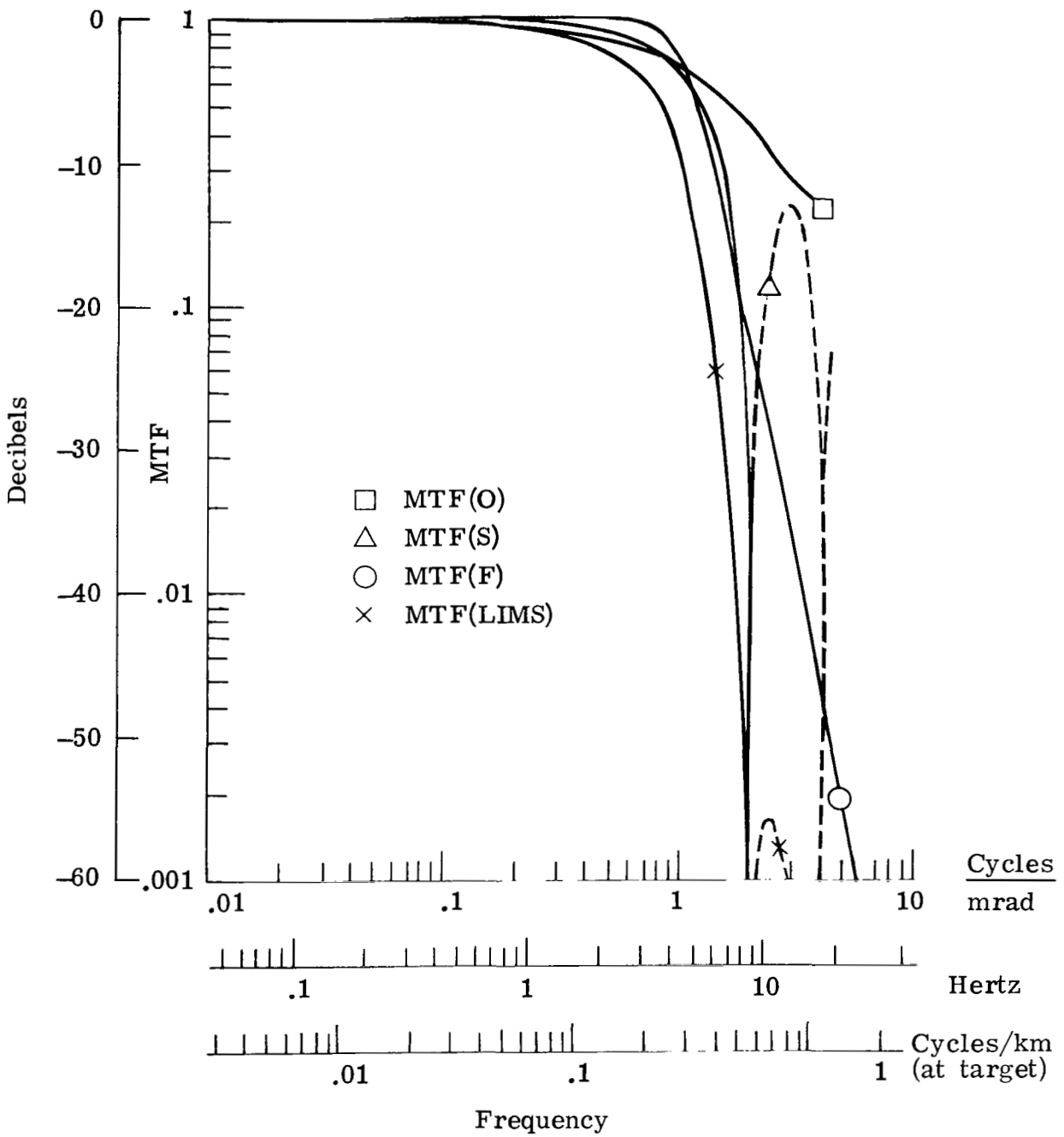

Figure C10.- Frequency response of LIMS radiometer for CO_2(narrow) channel. Dashed curve indicates spurious resolution.

APENDIX D

OPTIMIZATION OF FOCAL PLANE FOR OPTICAL TRANSFER FUNCTION CALCULATIONS

All the optical transfer function (OTF) calculations on the LIMS optical system that are presented in figures 5 and 6 and figures C1 to C6 were obtained for the best focus. The best focus is defined as the focal plane for which the modulation transfer function (MTF) data for all the detectors are most nearly maximum for a selected spatial frequency. The spatial frequency chosen was that equal to the reciprocal of twice the detector mask width (y dimension). For the NO_2 and H_2O detectors, the reference spatial frequency is 0.5 cycle/mrad, and for the other four detectors it is 1 cycle/mrad. For a given detector, this spatial frequency is one-half the first cutoff in the field-mask (slit) transfer function. (See figs. 8 and 9.)

Figure D1 shows the MTF, calculated for the reference spatial frequencies previously cited, as a function of focal position (z-direction) for all the detectors, as determined with the POLYPAGOS program and verified with the ACCOS V program. It can be seen that the best-focus choice (zero z position, abscissa of fig. D1) is a slight compromise among the six detectors. However, the 20- to 30-μm variation in best focus among the six detectors represents only about 2 units of variation in MTF (i.e., 2 percent of the zero-frequency value).

Figure D2 presents a further verification of the best focus choice, which is determined by using a POLYPAGOS subroutine to calculate the percentage of the radiant power from a point-source object, in an appropriate field position, that is available at each detector (ordinate). The zero z point (abscissa) in this figure is chosen identical to that in figure D1. The peaks on all these curves lie within 20 μm of the chosen best focus, and the peak MTF value for any curve is not different from the value at $z = 0$ by more than 1 percent of the zero-frequency MTF value. Note that the ordinate scale in figure D2 is expanded relative to that in figure D1.

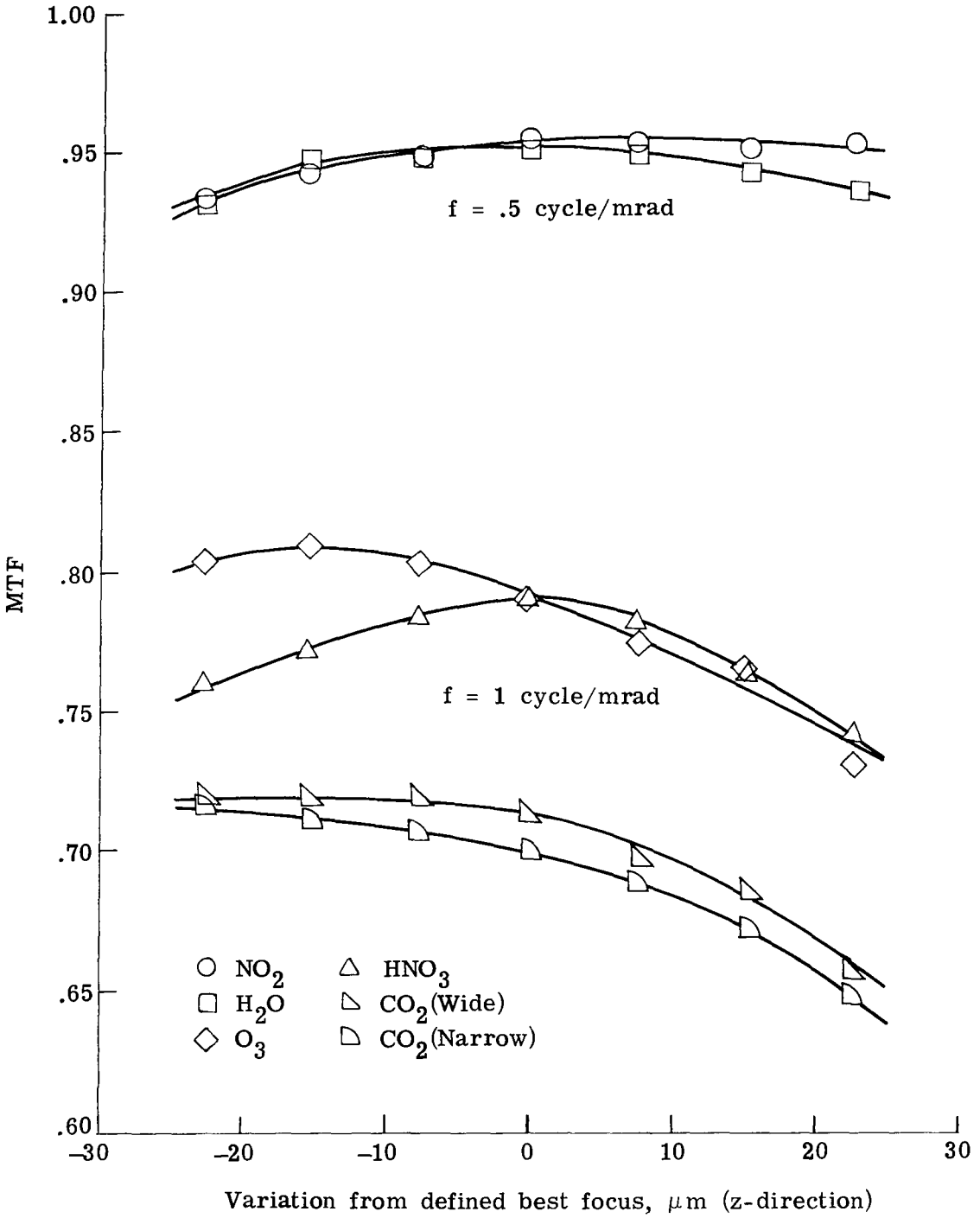

Figure D1.- MTF as a function of focus.

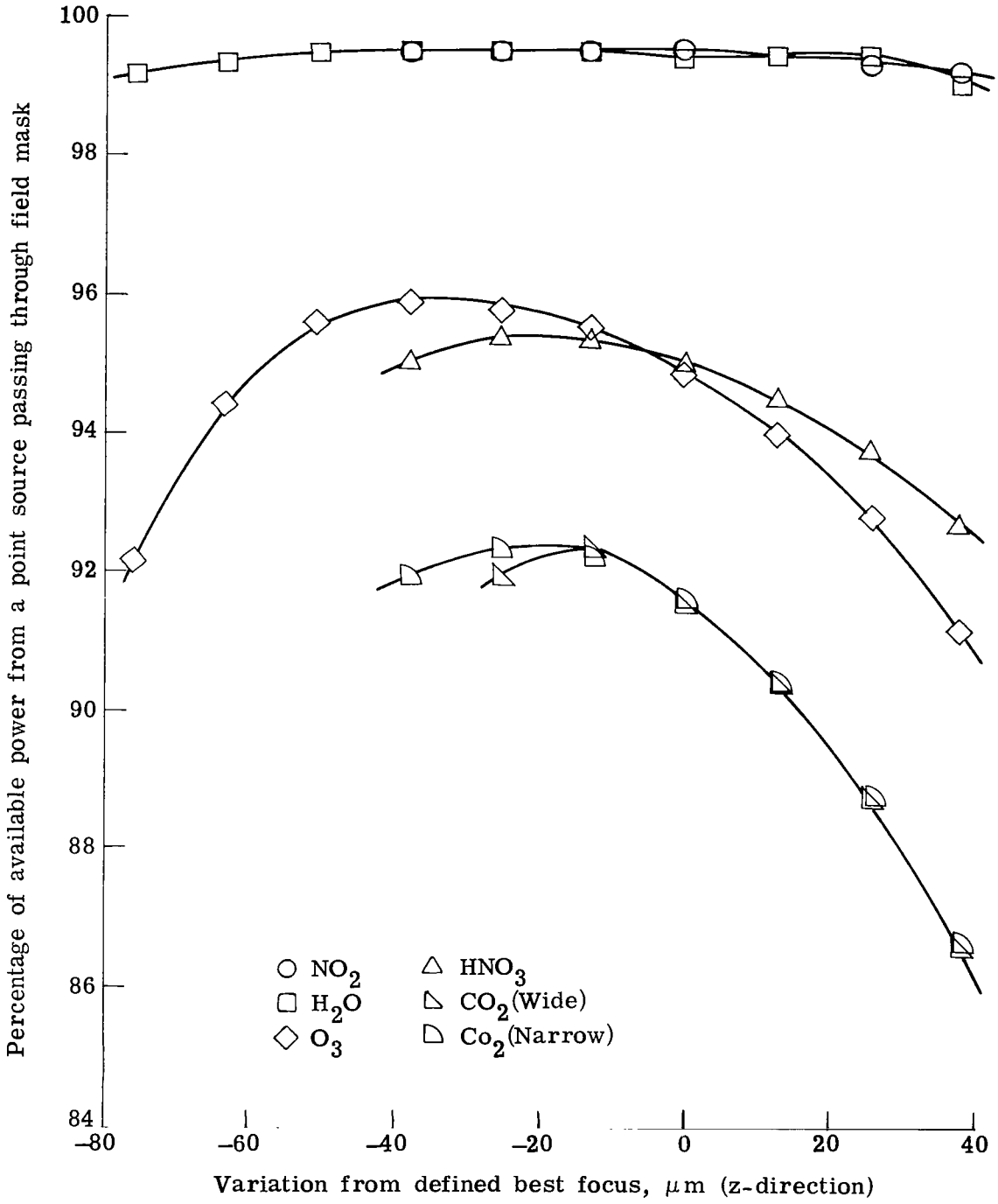

Figure D2.- Detector irradiance as a function of focus.

REFERENCES

1. Gille, John C.; and House, Frederick B.: On the Inversion of Limb Radiance Measurements I: Temperature and Thickness. J. Atmos. Sci., vol. 28, no. 8, Nov. 1971, pp. 1427-1442.

2. Gille, John C.; and Bailey, Paul L.: Inversion of Infrared Limb Emission Measurements for Temperature and Trace Gas Concentrations. Inversion Methods in Atmospheric Remote Sounding, Adarsh Deepak, ed., NASA CP-004, 1977, pp. 195-213.

3. Abel, Irving V.: Sensors for Atmospheric Measurement. Opt. Eng., vol. 17, no. 1, Jan./Feb. 1978, p. 5.

4. Harries, J. E.: The Distribution of Water Vapor in the Stratosphere. Rev. Geophys. & Space Phys., vol. 14, no. 4, Nov. 1976, pp. 565-575.

5. Drozewski, Richard W.; and Hatch, Marcus R.: Limb Infrared Monitor of the Stratosphere (LIMS) Experiment. Opt. Eng., vol. 17, no. 1, Jan./Feb. 1978, pp. 14-22.

6. Bates, Jerry C.; Hanson, David S.; House, Fred B.; Carpenter, Robert O'B.; and Gille, John C.: The Synthesis of 15μ Infrared Horizon Radiance Profiles From Meteorological Data Inputs. NASA CR-724, 1967.

7. Thomas, John R.; Jones, Ennis E.; Carpenter, Robert O'B.; and Ohring, George: The Analysis of 15μ Infrared Horizon Radiance Profile Variations Over a Range of Meteorological, Geographical, and Seasonal Conditions. NASA CR-725, 1967.

8. Williamson, W. R.; Shafer, D. R.; and Dilworth, D. C.: Lower Atmosphere Composition and Temperature Experiment. Opt. Eng., vol. 13, no. 4, July/Aug. 1974, pp. 303-306.

9. Drozewski, R. W.; Gille, J. C.; Thomas, J. R.; Twohig, K. J.; and Boyle, R. R.: Limb Radiance Inversion Radiometer. NASA CR-143712, 1975.

10. Otnes, Robert K.; and Enochson, Loren: Digital Time Series Analysis. John Wiley & Sons, c.1972.

11. Bendat, Julius S.; and Piersol, Allan G.: Random Data: Analysis and Measurement Procedures. John Wiley & Sons, Inc., c.1971.

12. Norton, Clarice L.; Brock, Gerald C.; and Welch, Roy: Optical and Modulation Transfer Functions. Photogramm. Eng. & Remote Sensing, vol. XLIII, no. 5, May 1977, pp. 613-636.

13. Brewer, Silas: POLYPAGOS: Polychromic Program for the Analysis of General Optical Systems. SAMSO-TR-70-411, U.S. Air Force, Sept. 1970. (Available from DDC as AD 715 262.)

14. ACCOS V On-Line Optics Design - User's Guide. National CSS, Inc., Sept. 1973.

15. Image Assessment & Specification. Volume 46 of Proceedings of Society of Photo-Optical Instrumentation Engineers, David Dutton, ed., c.1974.

16. Specification and Evaluation of Optical Systems. Opt. Acta, vol. 22, no. 4, Apr. 1975, pp. 242-390.

17. Stoelzner, William E.: Application of Fourier Techniques to Image Evaluation. SAMSO-TR-71-20, U.S. Air Force, Oct. 1970. (Available from DDC as AD 718 095.)

18. Parsons, John R.: Sampling Functions and Their Effect in Optical Systems Evaluation. SAMSO-TR-71-78, U.S. Air Force, Dec. 1970. (Available from DDC as AD 724 626.)

19. Goodman, Joseph W.: Introduction to Fourier Optics. McGraw-Hill Book Co., Inc., c.1968.

20. Gaskill, Jack D.: Linear Systems, Fourier Transforms, and Optics. John Wiley & Sons, c.1978.

TABLE I.- LIMS MEASURED FREQUENCY RESPONSE

LIMS channel (species)	Square-wave response at frequency, cycles/mrad, of -								
	0	0.1	0.2	0.4	0.6	0.7	0.8	1.0	1.2
NO_2	1.0	1.100	1.047	0.694	0.18	-----	-----	-----	-----
N_2O	1.0	1.079	1.064	.728	.20	-----	-----	-----	-----
O_3	1.0	.992	1.039	.926	.771	0.682	0.580	0.338	0.159
HNO_3	1.0	1.035	1.079	.962	.758	.651	.524	.295	.122
CO_2 (wide)	1.0	1.007	1.017	.930	.739	.638	.541	.304	.149
CO_2 (narrow)	1.0	1.031	1.038	.958	.742	.623	.505	.282	.122

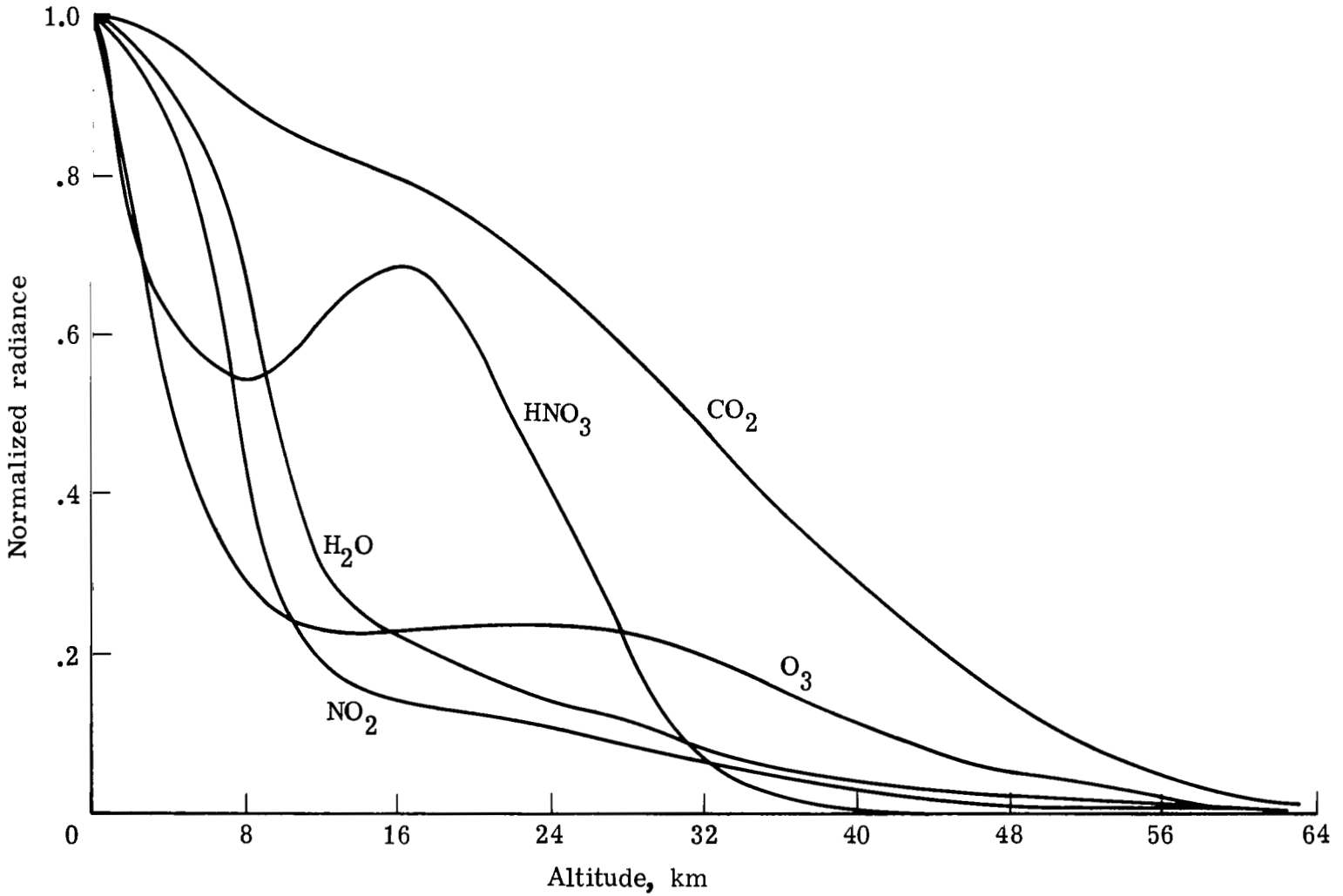

Figure 1.- Model radiance profiles of atmospheric constituent gases.

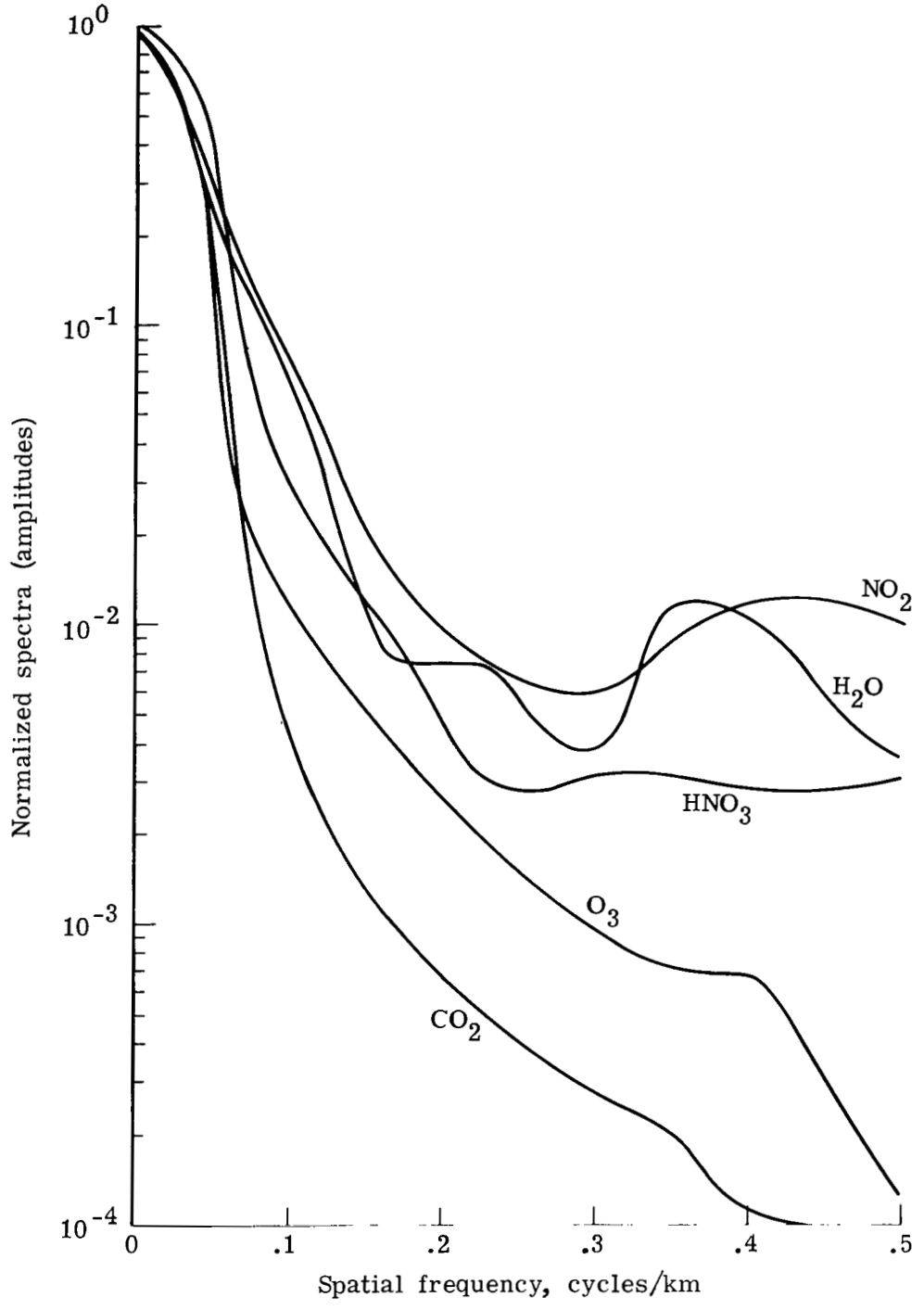

Figure 2.- Fourier input spectra for LIMS model radiance profiles.

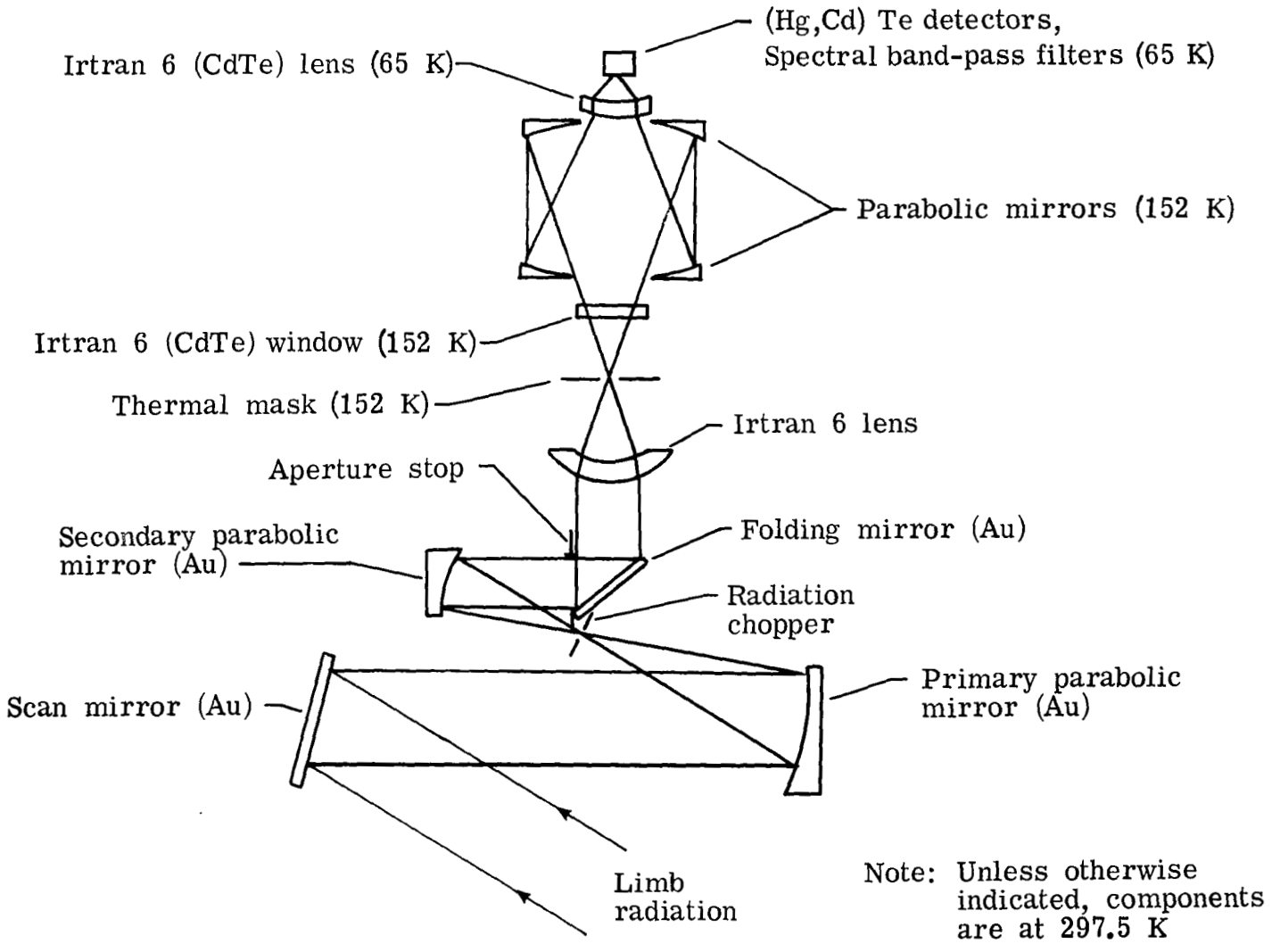

Figure 3.- LIMS optical schematic.

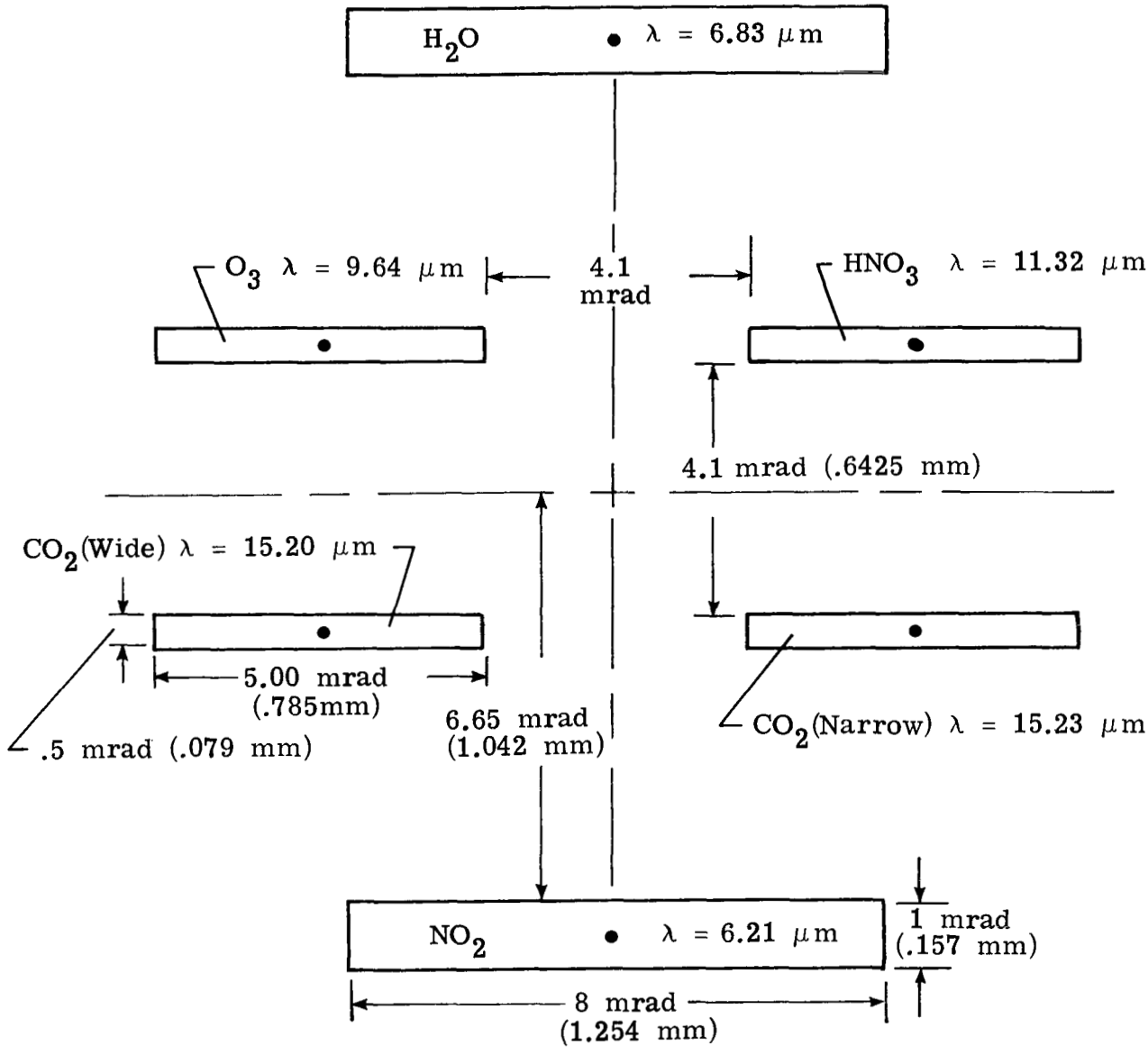

Figure 4.- Detector (field-of-view) mask and detectors. The black dots represent field points for OTF calculations and λ represents central wavelengths.

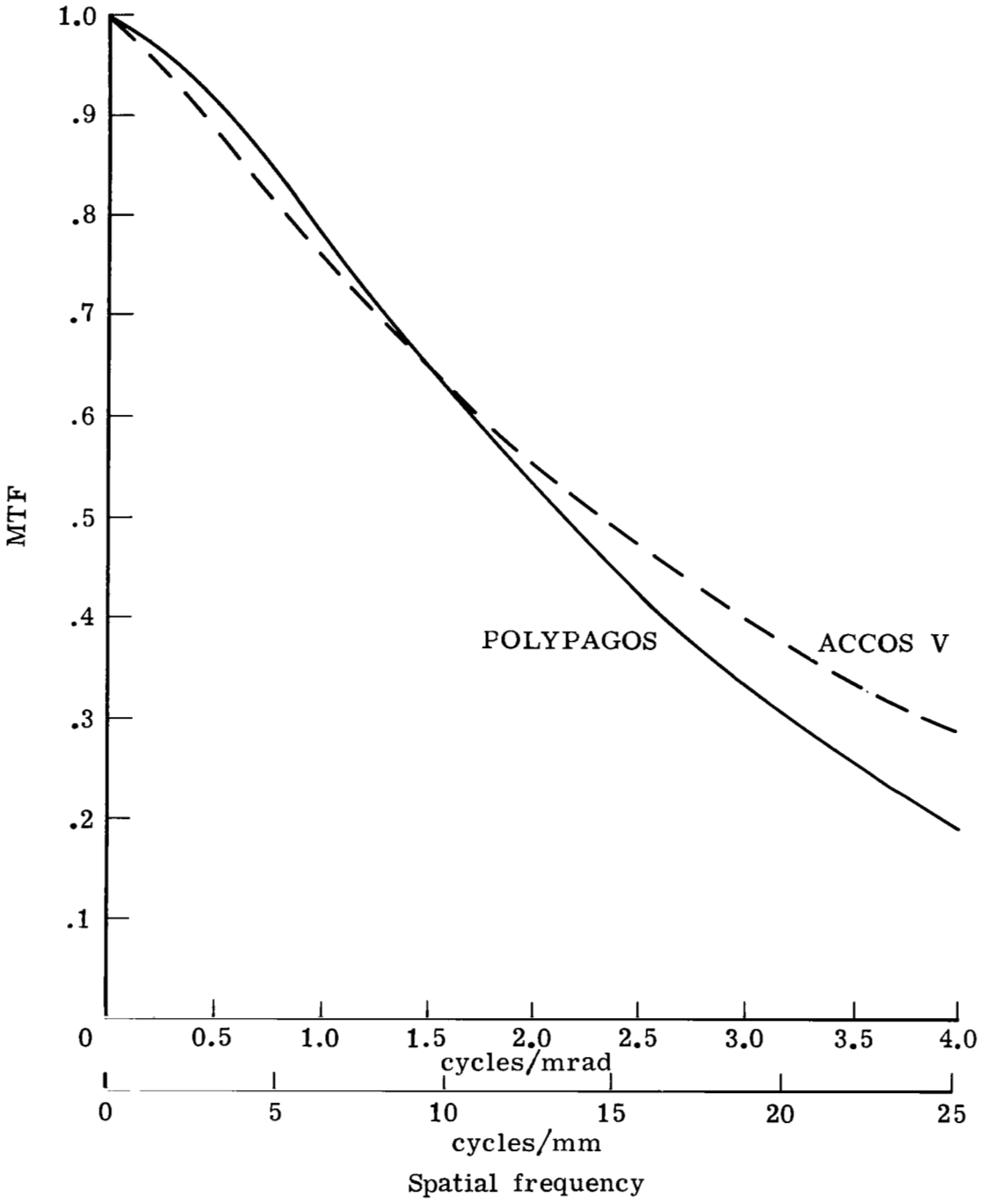

Figure 5.- MTF(optics) of LIMS O_3 channel.

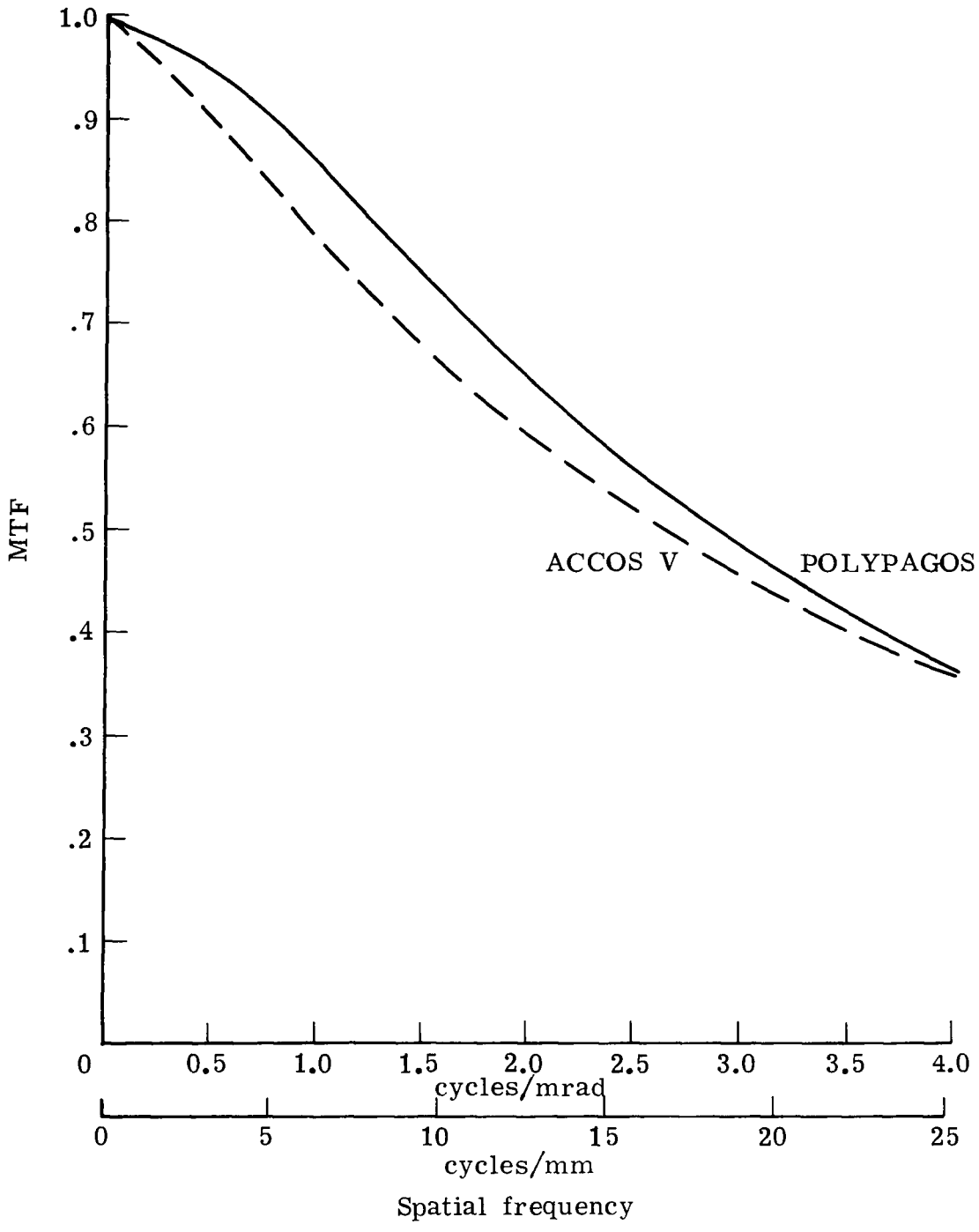

Figure 6.- MTF(optics) of LIMS H_2O channel.

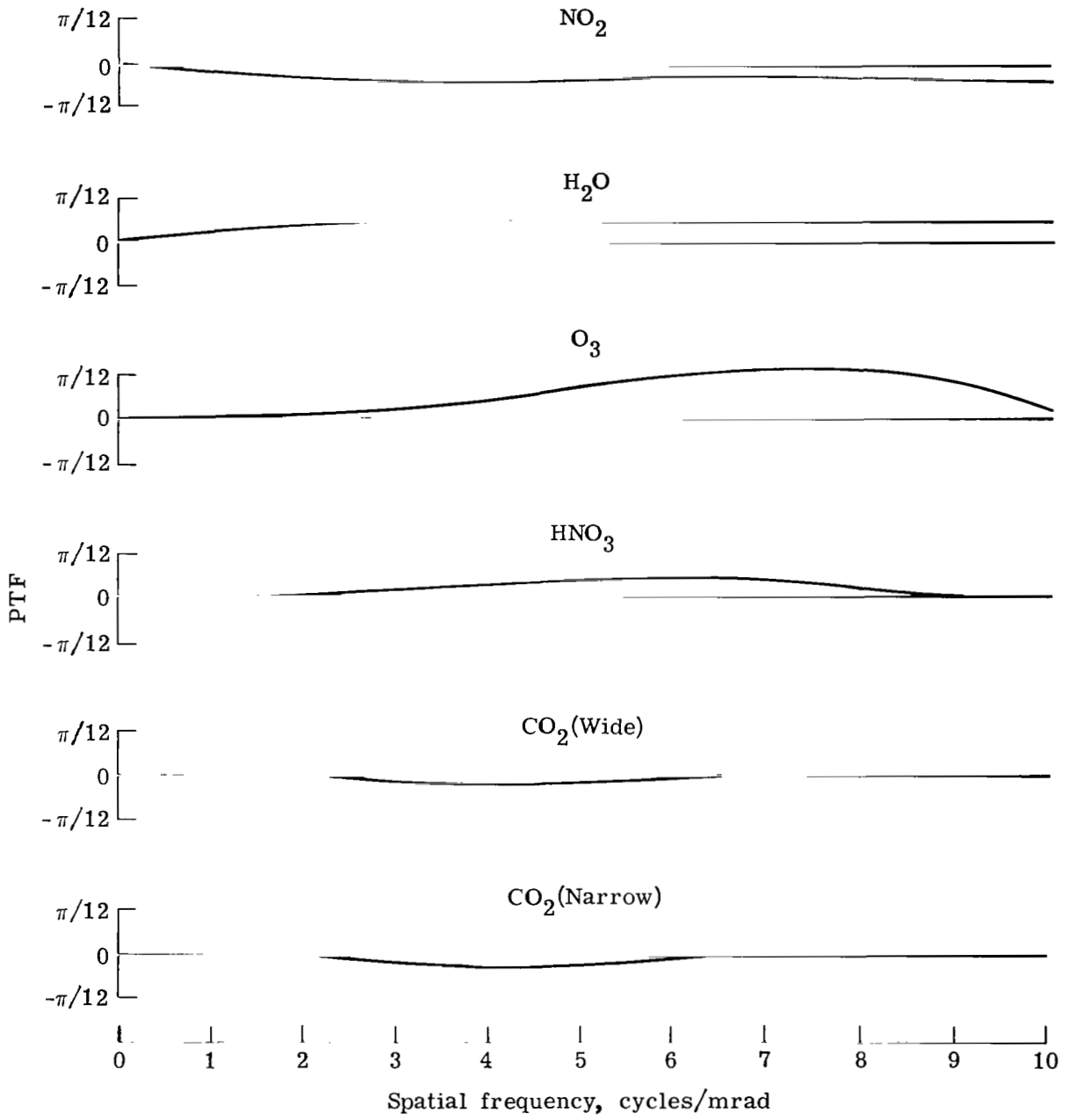

Figure 7.- Phase transfer function (PTF) of LIMS optics.

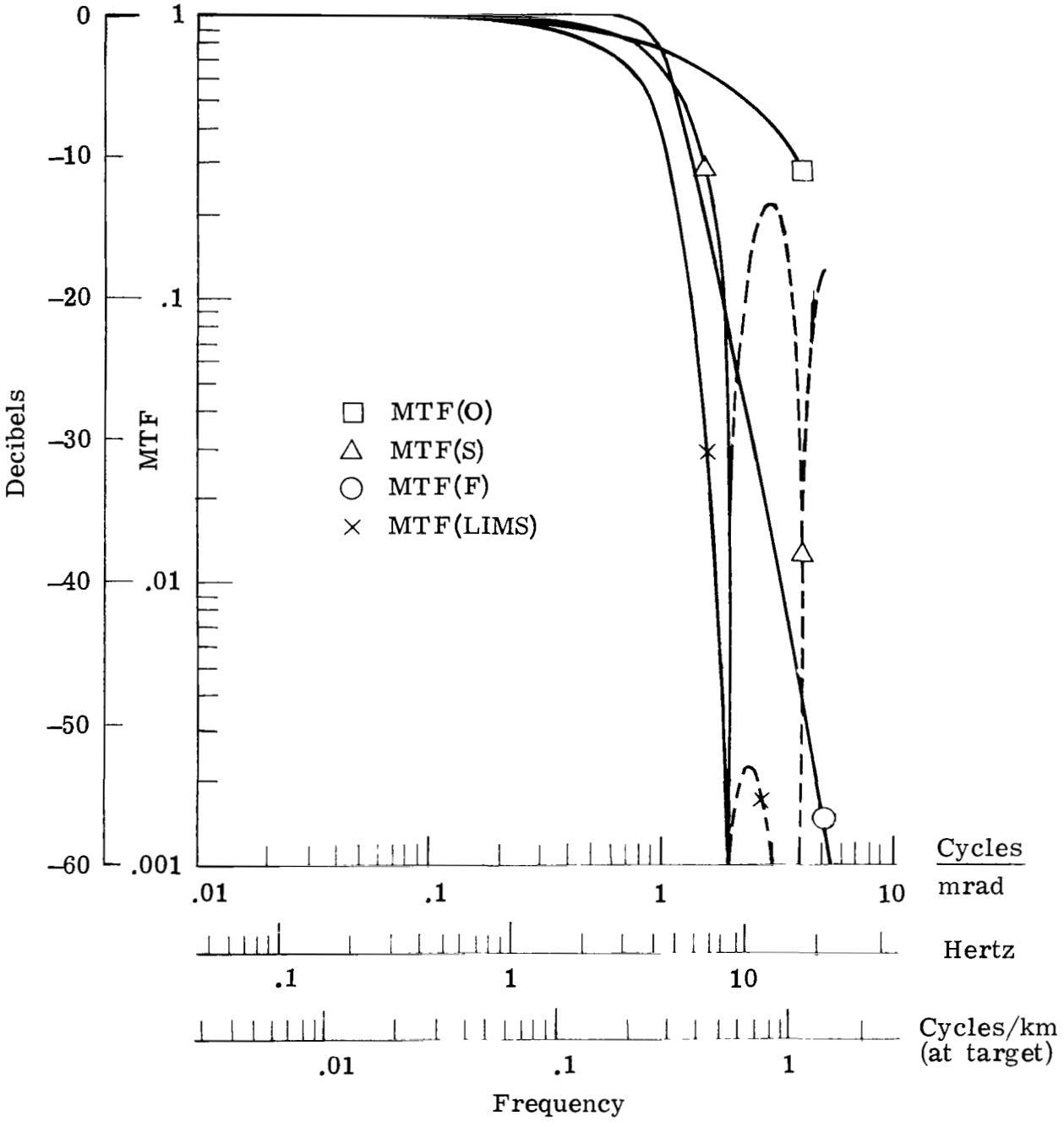

Figure 8.- Frequency response of LIMS radiometer for O_3 channel. (Desired pass band is 0.0 to 0.2 cycle/km.) Dashed curve indicates spurious resolution.

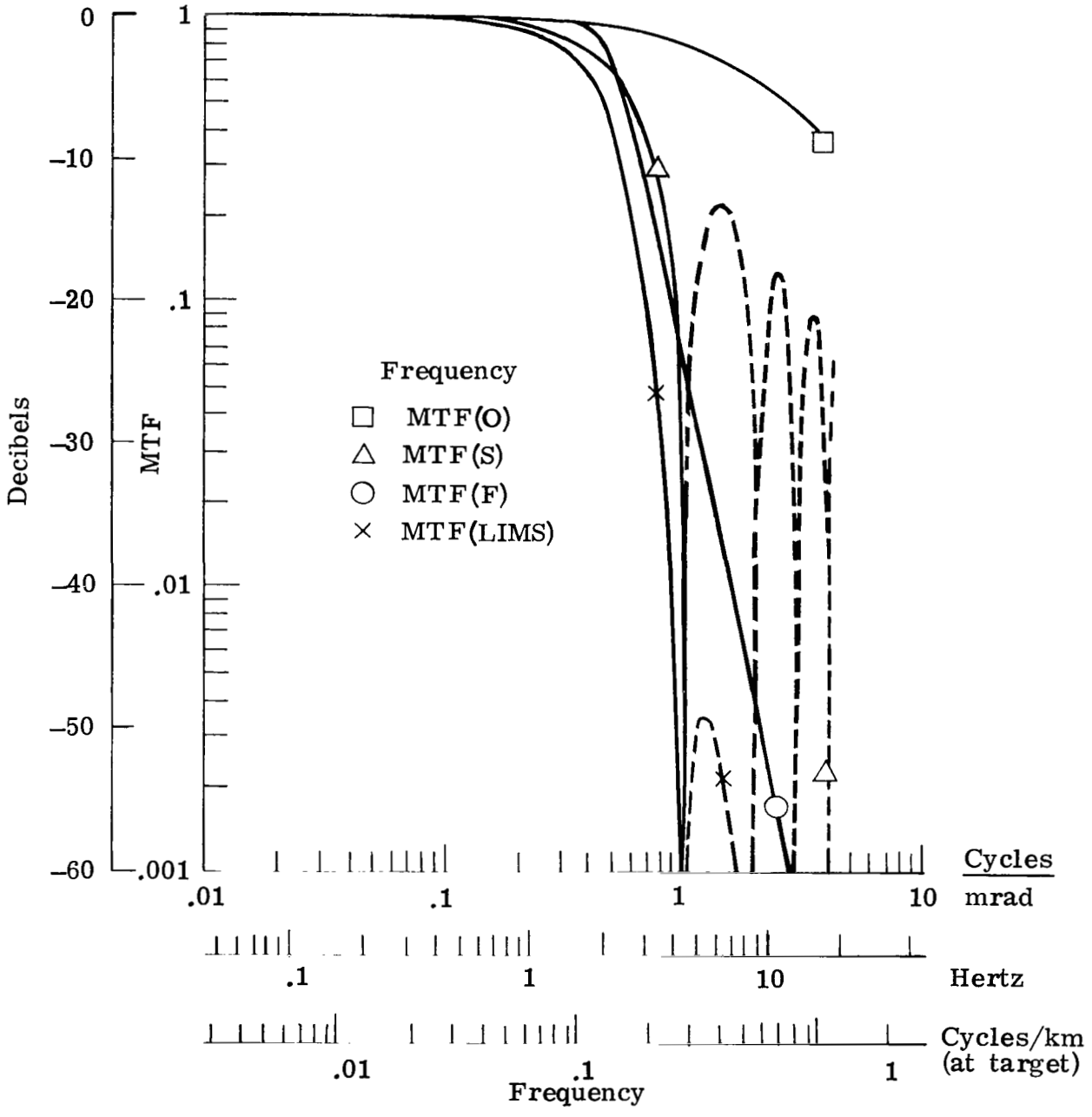

Figure 9.- Frequency response of LIMS radiometer for H_2O channel. (Desired pass band is 0.0 to 0.1 cycle/km.) Dashed curve indicates spurious resolution.

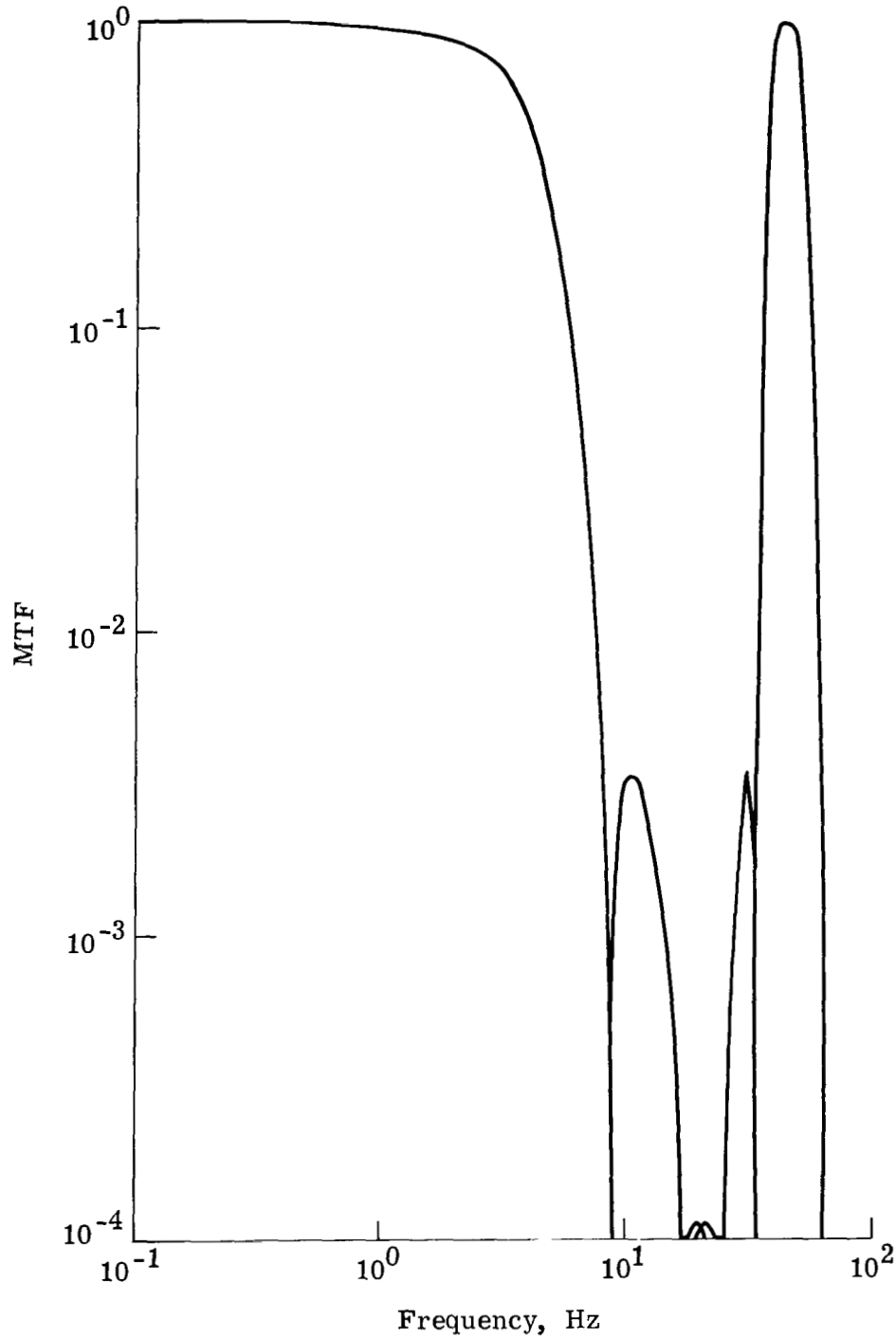

Figure 10.- Fundamental and first side band of sampling response. (Desired pass is 0.0 to 0.2 cycle/km.)

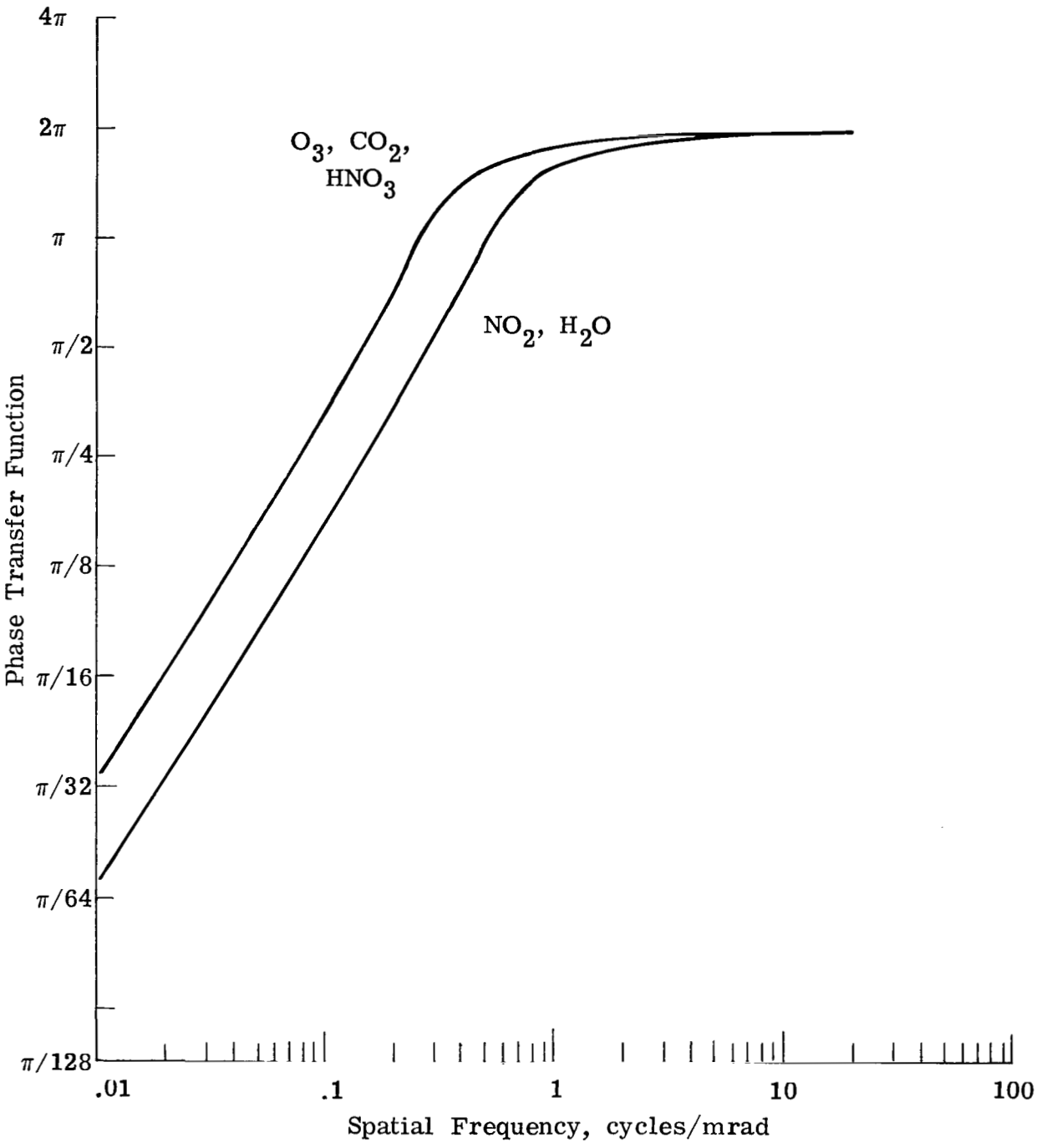

Figure 11.- Phase transfer function of LIMS radiometer.

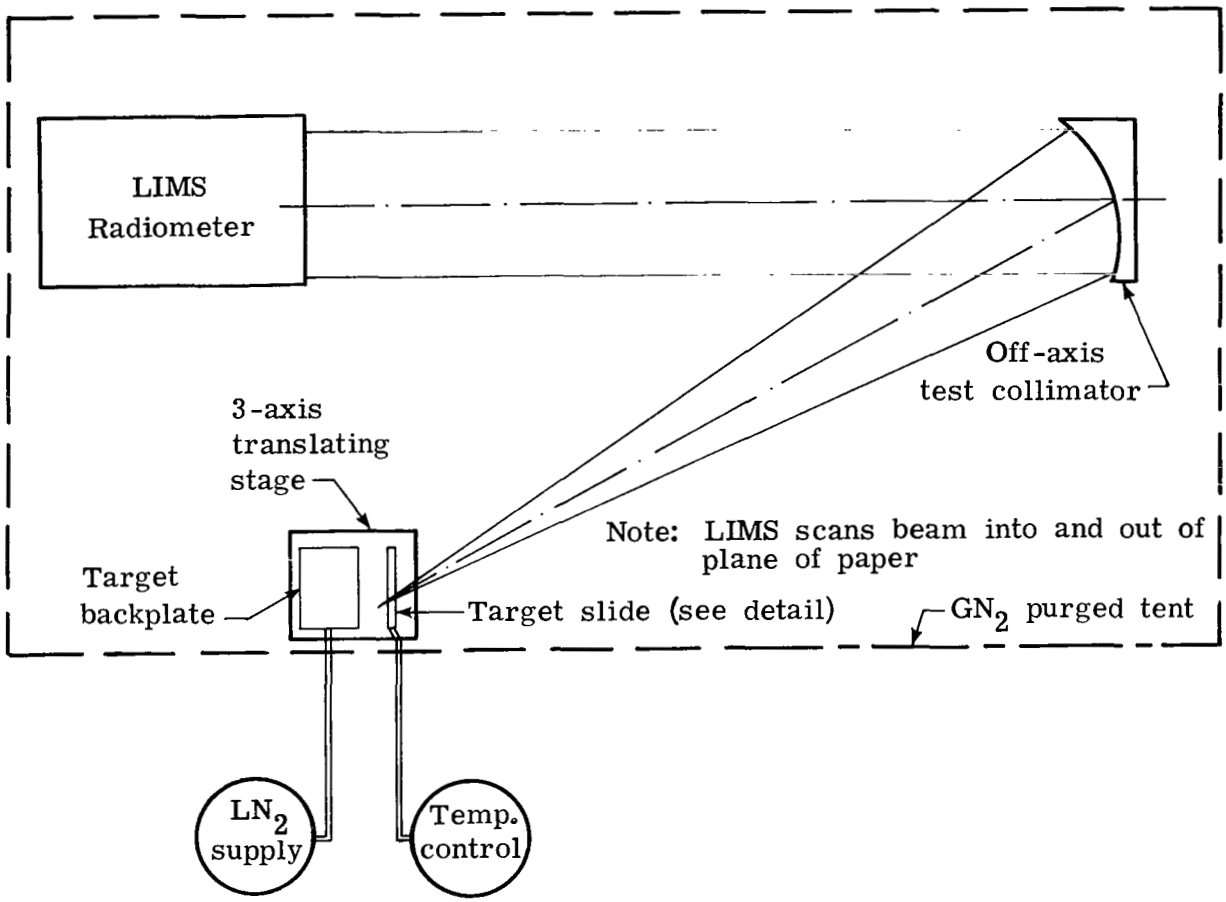

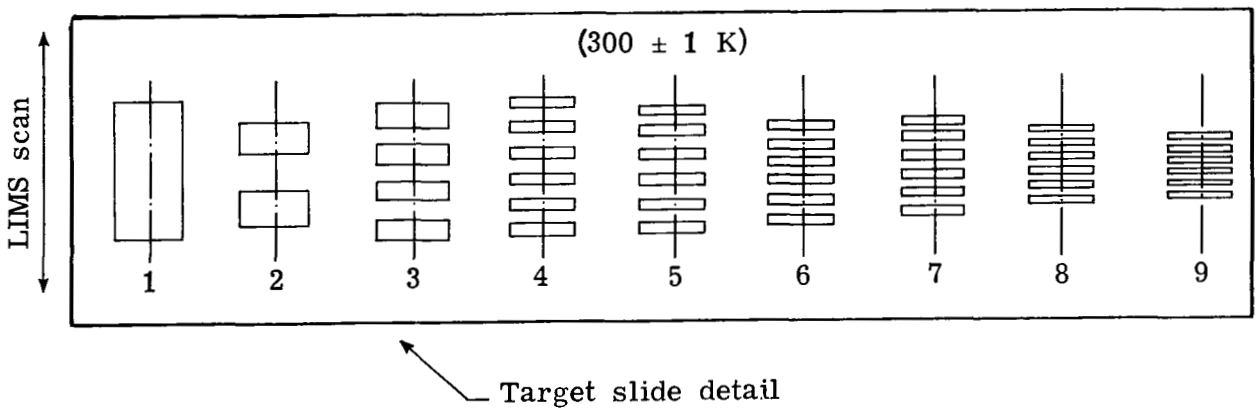

Figure 12.- MTF test configuration.

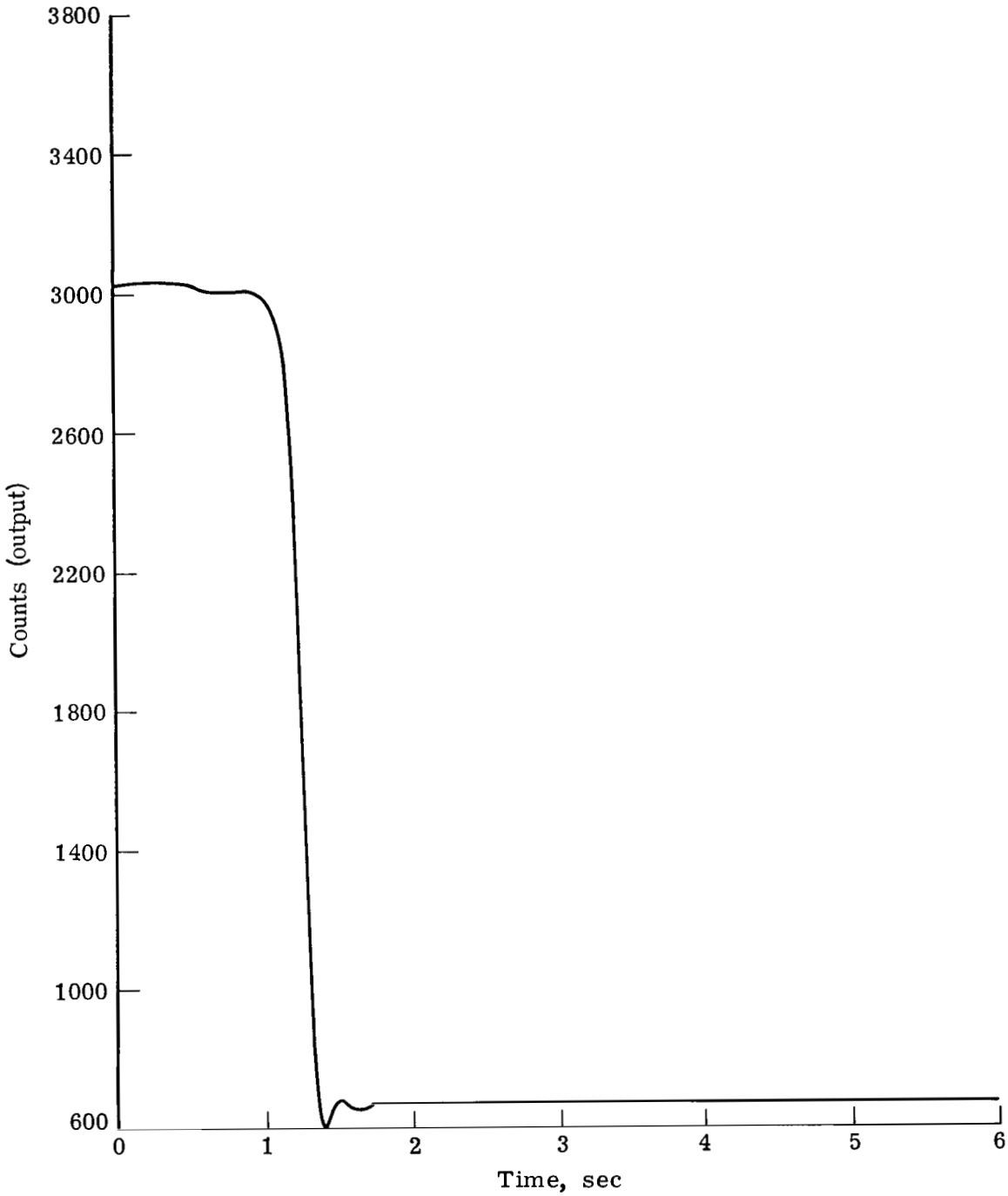

(a) Target segment 1.

Figure 13.- LIMS output of MTF test.

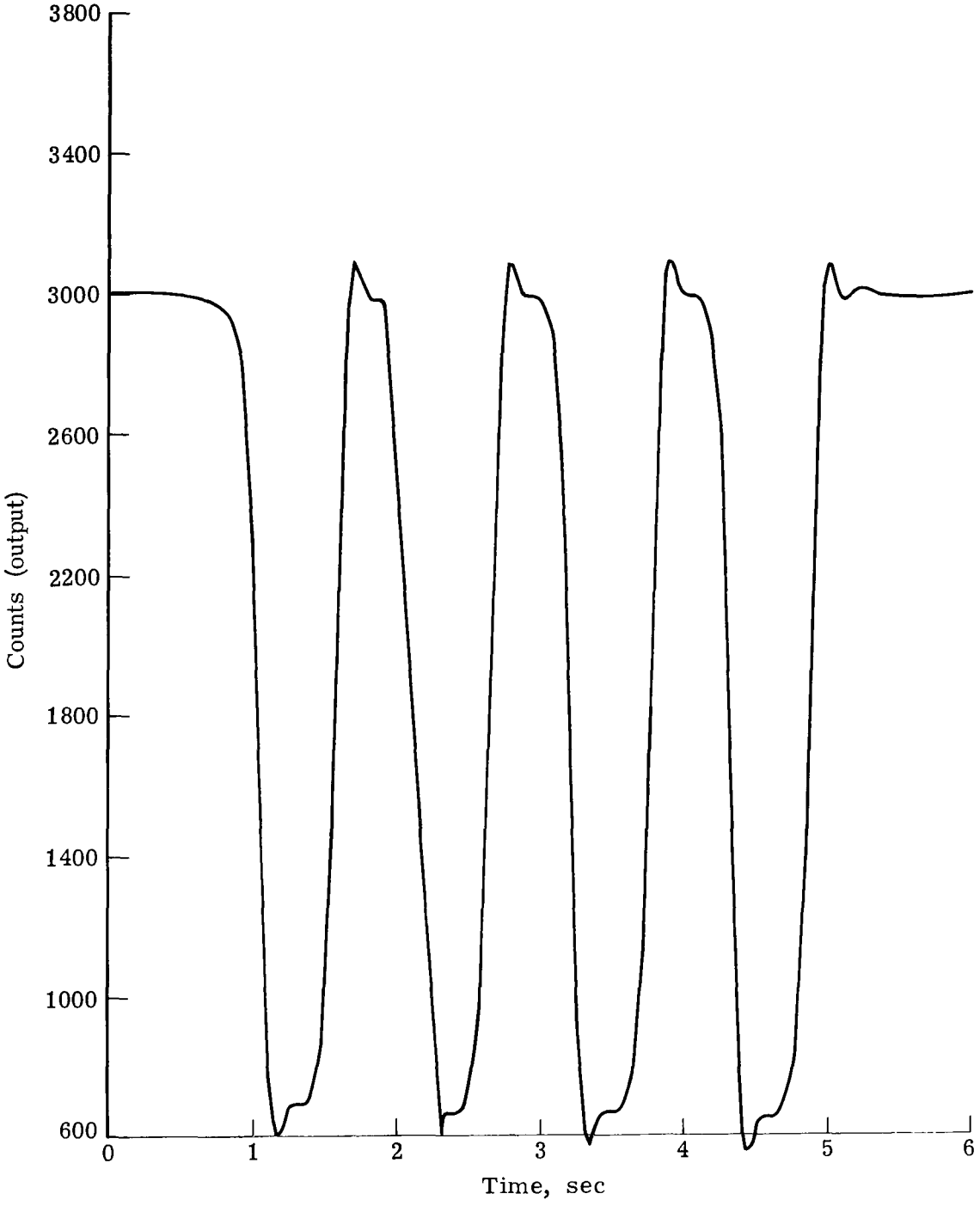

(b) Target segment 3.

Figure 13.- Continued.

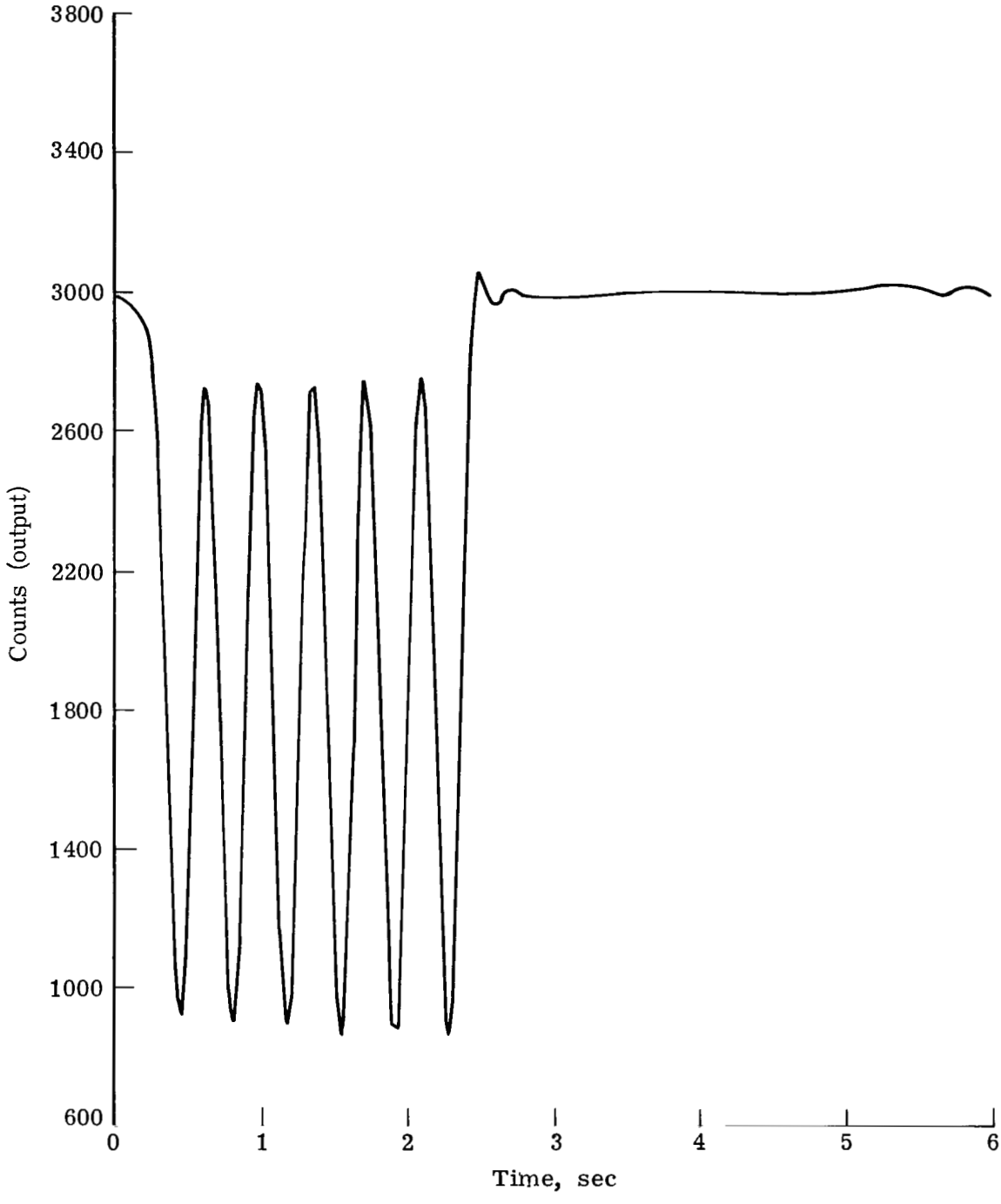

(c) Target segment 5.

Figure 13.- Concluded.

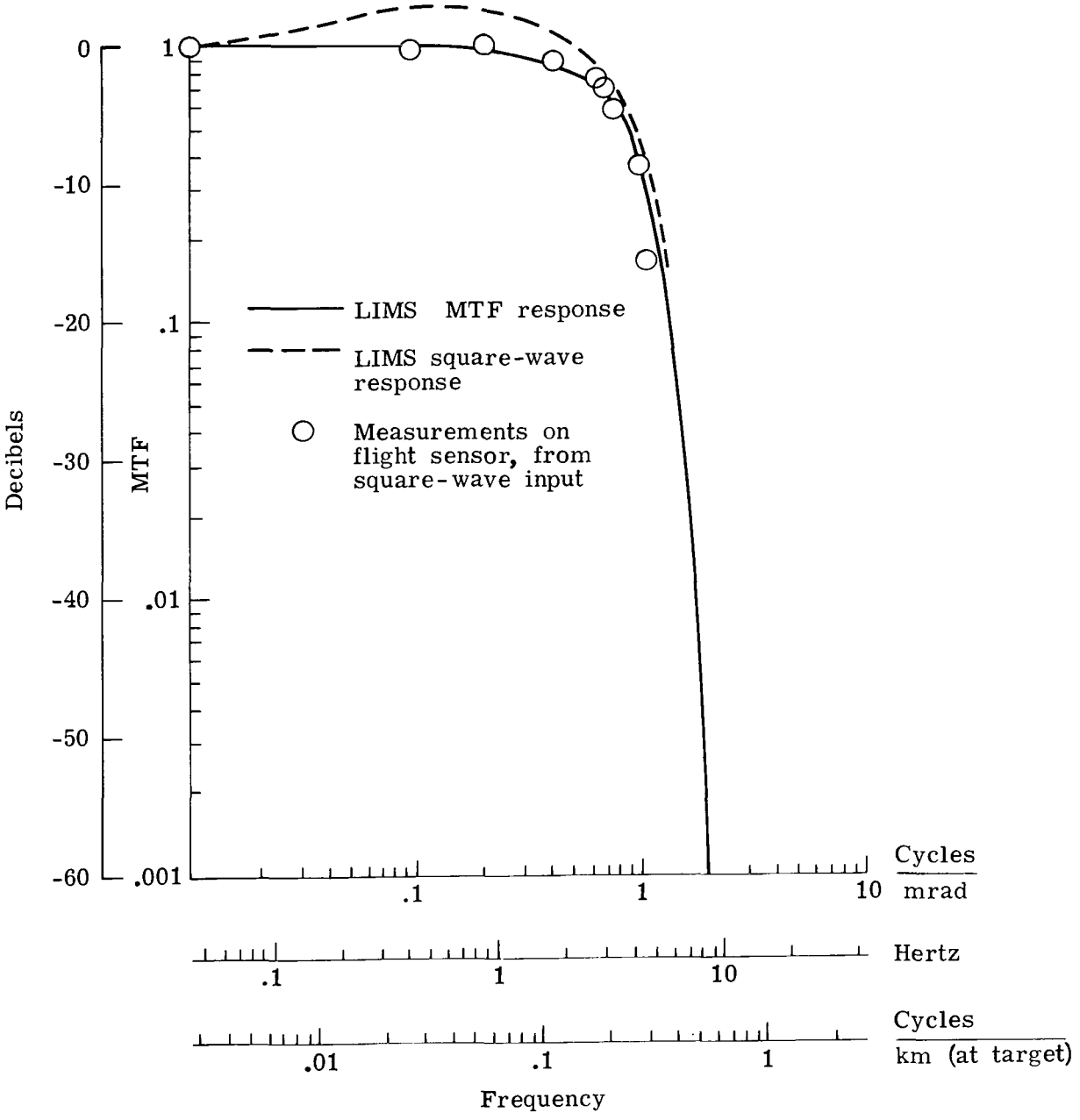

Figure 14.- Frequency response of LIMS radiometer for O_3 channel.

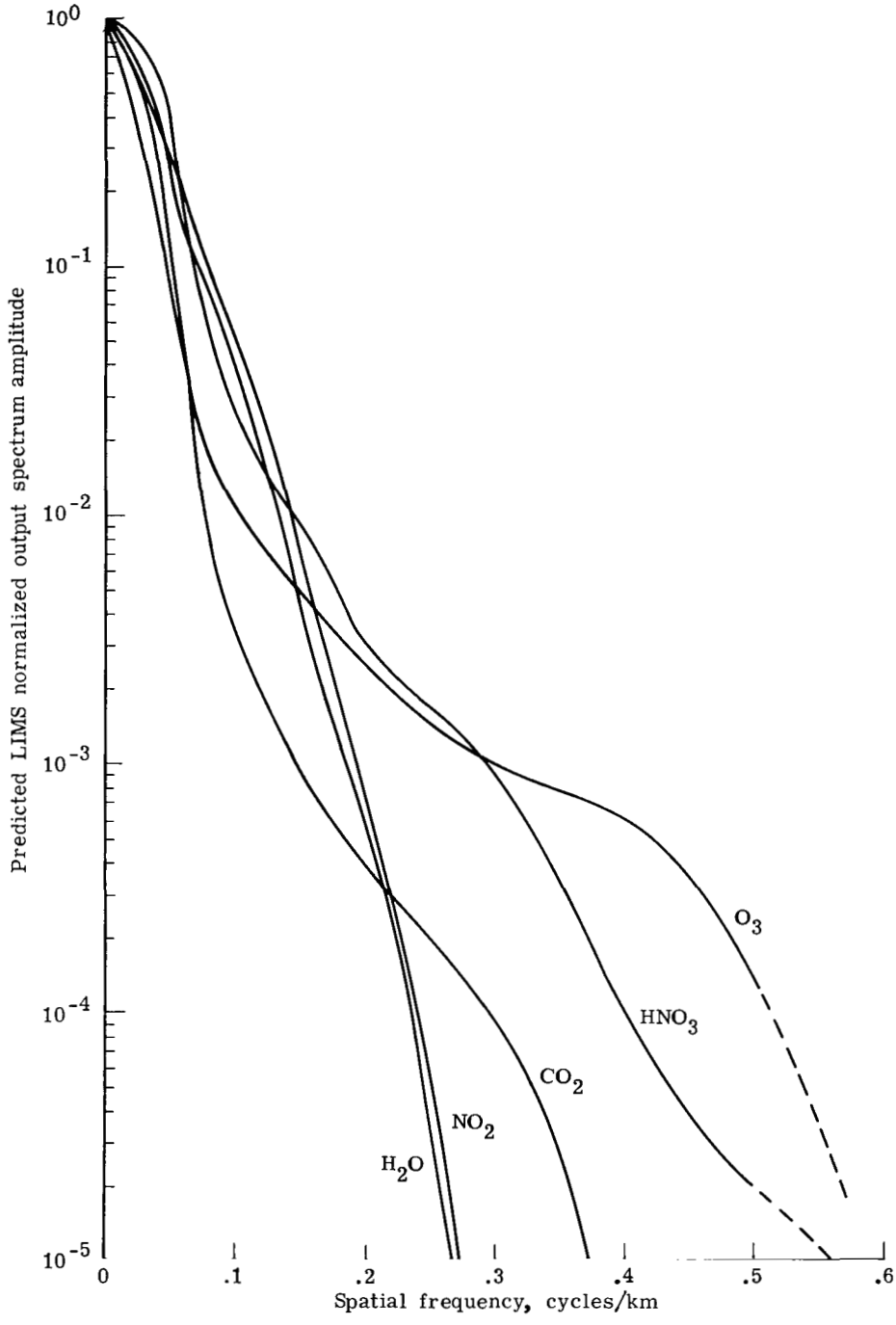

Figure 15.- Prediction of LIMS spectral output. Dashed line indicates extrapolation of data.

1. Report No.	2. Government Accession No.	3. Recipient's Catalog No.
NASA TP-1504		

4. Title and Subtitle

SPATIAL-FREQUENCY RESPONSE OF THE LIMB INFRARED MONITOR OF THE STRATOSPHERE

5. Report Date: August 1979

6. Performing Organization Code

7. Author(s)

R. Gale Wilson, Anthony Jalink, Jr., and William M. Kahlbaum, Jr.

8. Performing Organization Report No.: L-13037

10. Work Unit No.: 642-12-11-01

9. Performing Organization Name and Address

NASA Langley Research Center
Hampton, VA 23665

11. Contract or Grant No.

13. Type of Report and Period Covered: Technical Paper

12. Sponsoring Agency Name and Address

National Aeronautics and Space Administration
Washington, DC 20546

14. Sponsoring Agency Code

15. Supplementary Notes

16. Abstract

The Limb Infrared Monitor of the Stratosphere (LIMS) is one of the experiments on the Nimbus-7 satellite. It is designed to scan the Earth's limb vertically and to measure spectral emission profiles of trace atmospheric gases that are believed to be important in processes controlling the stratospheric ozone distribution. The LIMS must have adequate spatial-frequency response for all the spectral channels to provide, through inversion of the measured limb radiance profiles, important information about the temperature, structure, and composition of the atmosphere. Experiment objectives are reviewed and several analyses and measurements are described which were performed to determine the adequacy of the system for satisfying these objectives. From the LIMS design-model data, the modulation transfer function (MTF) was calculated for the optical system, the detector field mask, the electronics, and the overall system for each channel. The signal output performance of the instrument was predicted from the system MTF data and model input radiance data for each channel. The MTF measurements made on the flight sensor confirmed the analytical results. The predictions indicate that the instrument can satisfy the basic measurement objectives of the experiment.

17. Key Words (Suggested by Author(s))

Infrared
Air pollution
Atmosphere
Spatial-frequency response
Stratosphere
Limb

18. Distribution Statement

Unclassified - Unlimited

Subject Category 45

19. Security Classif. (of this report)	20. Security Classif. (of this page)	21. No. of Pages	22. Price*
Unclassified	Unclassified	49	$4.50

* For sale by the National Technical Information Service, Springfield, Virginia 22161

NASA-Langley, 1979

13 1 1U,E, 080679 S00903DS
DEPT OF THE AIR FORCE
AF WEAPONS LABORATORY
ATTN: TECHNICAL LIBRARY (SUL)
KIRTLAND AFB NM 87117